Reproducibility and variability of earthquake subsidence estimates from saltmarshes of a Cascadia estuary

JASON S. PADGETT,[1,2,3]* SIMON E. ENGELHART,[1] HARVEY M. KELSEY,[4] ROBERT C. WITTER[5] and NIAMH CAHILL[6]

[1]Department of Geography, Durham University, Durham, DH1 3LE, UK
[2]Department of Geosciences, University of Rhode Island, Kingston, Rhode Island, 02881, USA
[3]U.S. Geological Survey, Pacific Coastal Marine Science Center, Santa Cruz, California, 95060, USA
[4]Department of Geology, Cal Poly Humboldt, 1 Harpst Street, Arcata, 95521, USA
[5]U.S. Geological Survey, Alaska Science Center, Anchorage, Alaska, 99508, USA
[6]Department of Mathematics and Statistics, Maynooth University, Kildare, Ireland

ABSTRACT: We examine fossil foraminiferal assemblages from 20 sediment cores to assess sudden relative sea-level (RSL) changes across three mud-over-peat contacts at three salt marshes in northern Humboldt Bay, California (~44.8°N, −124.2°W). We use a validated foraminiferal-based Bayesian transfer function to evaluate the variability of subsidence stratigraphy at a range of 30-6000 m across an estuary. We use the consistency in RSL reconstructions to support estimates of coseismic subsidence from megathrust earthquakes. To assess the variability of subsidence estimates, we analyzed: nine examples of the 1700 CE earthquake (average of 0.64 ±0.14 m subsidence; range of 0.24 ± 0.27 to 1.00 ± 0.44 m), five examples of the ca. 875 cal a BP earthquake (average of 0.43 ±0.16 m; range of 0.41 ± 0.36 to 0.48 ± 0.39 m), and six examples of the ca. 1120 cal a BP earthquake (average of 0.70±0.18 m; range of 0.47 ± 0.36 to 0.80 ± 0.49 m). Our subsidence estimates suggest ~±0.3 m of within-site (intrasite) variability, which is consistent with previous research. We also identify inconsistencies between sites (intersite) at northern Humboldt Bay greater than one-sigma uncertainties, driven by variable foraminiferal assemblages in the mud overlying the 1700 CE subsidence contact. Therefore, we recommend at least two quantitative microfossil reconstructions across the same stratigraphic sequence from different marsh sites within an estuary to account for estimate variability and provide increased confidence in vertical coseismic deformation estimates. Our results have broad implications for quantitative, microfossil-based reconstructions of coseismic subsidence at temperate coastlines globally. © 2022 The Authors. *Journal of Quaternary Science* Published by John Wiley & Sons Ltd.

KEYWORDS: paleogeodesy; relative sea level; Cascadia; tidal wetland stratigraphy; megathrust paleoseismology

INTRODUCTION

Stratigraphy consisting of abrupt mud-over-peat and mud-over-upland soil contacts are the most common signature of coseismic subsidence associated with megathrust deformation in temperate coastal environments (Atwater, 1987; Combellick, 1991; Nelson 1992; Shennan et al., 1996, 1999; Sawai et al., 2002; Cisternas et al., 2005). Early coastal palaeogeodetic research revolutionised our understanding of subduction zone hazards by identifying and mapping wetland stratigraphy consistent with megathrust rupture and estimating coseismic vertical deformation across subsidence contacts based on qualitative or cluster-based quantitative elevation assignments of palaeodepositional environments (Plafker, 1969; Atwater, 1992; Nelson 1992, Nelson et al., 1996a, b; Darienzo et al., 1994; Shennan et al., 1996; Atwater and Hemphill-Haley, 1997) with large, uniformly distributed errors (>±0.5 m). However, subsequent refinement of relative sea level (RSL) reconstructions and increased precision of coseismic subsidence estimates using quantitative methods (transfer functions) can now help to better understand the complexities of past megathrust rupture such

as rupture length and variability of rupture magnitude (Guilbault et al., 1995, 1996; Hamilton and Shennan, 2005; Hawkes et al., 2010, 2011; Wang et al., 2013; Garrett et al., 2015; Milker et al., 2015, 2016; Shennan et al., 2016; Dura et al., 2017; Kemp et al., 2018; Nelson et al., 2020; Padgett et al., 2021). Along the coasts of the Cascadia subduction zone (CSZ), transfer functions based on fossil foraminiferal assemblages may yield precise (<±0.3 m) estimates of coseismic subsidence with normally distributed errors (Guilbault et al., 1995, 1996; Nelson et al., 2008; Hawkes et al., 2010; 2011; Engelhart et al., 2013a, Wang et al., 2013; Milker et al., 2016, Kemp et al., 2018; Nelson et al., 2020; Padgett et al., 2021).

Despite improvements in the precision of coseismic subsidence estimates over the past decade (Hawkes et al., 2010; Milker et al., 2015) and the validation of the foraminiferal transfer function approach at Cascadia (Engelhart et al., 2013a; Kemp et al., 2018), questions remain regarding the reproducibility of coseismic subsidence estimates, e.g. the depositional variability of an earthquake-induced stratigraphic sequence, and the role that depositional variability may have on microfossil assemblages. Over small areas (e.g. 1–5 km), several processes can cause subsidence estimates to deviate from the actual coseismic land-level change across the environment. Potential impacts

*Correspondence: Jason S. Padgett, Department of Geography, Durham University, Durham, DH1 3LE, UK.
Email: jpadgett@usgs.gov

of these processes on microfossils and, subsequently, the accuracy of coseismic subsidence estimates can include post-depositional modification of the assemblage (e.g. physical/biological mixing), microfossil assemblages providing elevation estimates that do not immediately bracket the time of coseismic subsidence (e.g. erosion of the former marsh surface or delay in resumption of sedimentation), and sedimentological processes that result in microfossils estimating the elevation change due to both coseismic subsidence and other processes (e.g. post-seismic deformation, compaction and/or liquefaction). Teasing apart these processes is difficult without extensive microfossil and sediment analyses. Further, the question of the appropriate sampling area (geospatial extent) to use in the determination of a coseismic subsidence estimate (e.g. within marsh, within estuary) remains unsolved. These unknowns are critical given the array of processes that vary across relatively small spatial scales and could influence a marsh-based coseismic subsidence estimate.

After extensive mapping of wetland stratigraphy, coastal palaeogeodetic investigations avoid subtle lithostratigraphic irregularities and select the sediment collection location that displays the most visually abrupt stratigraphic contact for microfossil analyses and derivation of a coseismic vertical deformation estimate. This estimate is then often assumed to be representative over an entire estuary, but without understanding the variability of subsidence estimates at the scale of an outcrop or across an estuary (Nelson et al., 1996a; Shennan et al., 2016). On a margin-wide scale, across multiple estuaries, foraminiferal-based transfer function investigations of the CSZ 1700 CE earthquake show that vertical deformation was non-uniform along the margin (e.g. Hawkes et al., 2011; Wang et al., 2013). However, the current CSZ 1700 CE palaeogeodetic database, of fossil foraminifera-based coseismic subsidence estimates, is comprised of only 15 sites along the margin and 13 of the sites have a single estimate. Therefore, small-scale lithostratigraphic and biostratigraphic preservation irregularities may have important implications for margin-wide palaeoseismic interpretations both at Cascadia and subduction zones globally.

To our knowledge, no work has focused on assessing the reproducibility of a microfossil-based transfer function over distances of 1–6 km across multiple tidal marshes in the same estuarine system, where second-order influences on stratigraphic evidence of coseismic land-level changes may not be uniform. To evaluate site-specific, estuary-wide, and regional systematic differences, it is necessary to identify the extent of lithostratigraphic and biostratigraphic variability across subsidence contacts. Here we use a validated Bayesian foraminiferal-based transfer function (BTF; Kemp et al., 2018) to test the physical consistency of subsidence reconstructions among closely spaced cores and sites, at northern Humboldt Bay, California (~44.8°N, -124.2°W). We assess variability within a study site (intrasite; spatial scales <1000 m) and within an estuary (intersite; spatial scales of 1–6 km). We examine three abrupt mud-over-peat (coseismic subsidence) contacts along a 6 km transect from Jacoby Creek, McDaniel Creek and Mad River Slough (Fig. 1). To evaluate the consistency of our estimates, we analysed 20 fossil sediment cores containing the three mud-over-peat contacts: nine examples of the 1700 CE contact, five examples of the ~875 cal a BP contact, and six examples of the ~1120 cal a BP contact. The main objectives of this investigation are to evaluate the variability of subsidence stratigraphy across an estuary and consider the best techniques to reduce the likelihood of deriving an unrepresentative estimate of coseismic vertical deformation.

STUDY AREA

Environmental setting

The two-lobed morphology of Humboldt Bay is the combined result of Quaternary tectonics and late Holocene RSL rise (Thompson, 1971; Vick, 1988; Clarke and Carver, 1992; Valentine, 1992). Northern Humboldt Bay coastal lowlands are protected from the Pacific Ocean by ~20–25 m high Lanphere-Ma-le'l Dunes (Fig. 1c; Vick, 1988; Pickart and Hesp, 2019). Within the estuary, several fringe salt-marsh environments formed along the periphery and proximate to small drainages but also on dissected islands (Eicher, 1987; Vick, 1988; Clarke and Carver, 1992; Valentine, 1992; Pritchard, 2004). From east to west, Jacoby Creek, McDaniel Creek and Mad River Slough are the largest tidal marshes within the northern Humboldt Bay estuary. A National Oceanic and Atmospheric Administration tide gauge station at the mouth of Mad River Slough documents a 2.36 m semi-diurnal tidal range (mean higher high water (MHHW) – mean lower low water). High marshes form at elevations around MHHW and low marshes form at elevations around mean high water (MHW; Pritchard, 2004). Floral communities within northern Humboldt Bay are consistent with typical Cascadia tidal wetland floral distributions (Pritchard, 2004; Hawkes et al., 2010; Kemp et al., 2018). In high-marsh environments, floral communities include Castilleja exserta, Distichlis spicata, Grindelia spp., Jaumea carnosa, Spartina densiflora and Triglochin maritimum (Eicher, 1987; Schlosser and Eicher, 2012). Floral communities of middle and lower marsh environments include Distichlis spicata, Salicornia virginica, Spartina densiflora and Triglochin maritimum (Eicher, 1987; Schlosser and Eicher, 2012).

Tidal wetland stratigraphy

In this study we leverage the palaeogeodetic investigation of Padgett et al. (2021) at the northern Humboldt Bay estuary. Padgett et al. (2021) mapped mud-over-peat and mud-over-upland soil contacts within the tidal wetland stratigraphy at Jacoby Creek, McDaniel Creek and Mad River Slough marshes. Based on depth in cores, radiocarbon age distributions, fossil foraminiferal analysis, and regional plate boundary age overlap comparisons, Padgett et al. (2021) observed four stratigraphic contacts consistent with coseismic subsidence caused by megathrust-earthquake rupture. At McDaniel Creek, diatom assemblages (Engelhart et al., 2016) and allochthonous foraminiferal assemblages suggest that the organic-rich unit underlying the deepest, ca. 1620 cal a BP, subsidence contact is an upland soil (Padgett et al., 2021). Therefore, this investigation focuses on the three most recent coseismic subsidence contacts in northern Humboldt Bay that occurred at 1700 CE, ca. 875 cal a BP and ca. 1120 cal a BP. Stratigraphic evidence for the ca. 875 cal a BP subsidence contact was absent at Jacoby Creek (Padgett et al., 2021). Within our analysis, we employ data from three foraminiferal RSL reconstructions from Padgett et al. (2021) supplemented with an additional 17 reconstructions.

RESEARCH APPROACH AND METHODS

Our research approach is three-fold: (1) lithostratigraphic analysis to evaluate subsidence contact stratigraphy based on visual appearance and density imagery; (2) RSL reconstructions and derivation of subsidence estimates to estimate palaeoenvironmental elevation changes using foraminiferal data and an existing BTF (Kemp et al., 2018); and (3) assess the intra- (within one site) and intersite (between multiple sites)
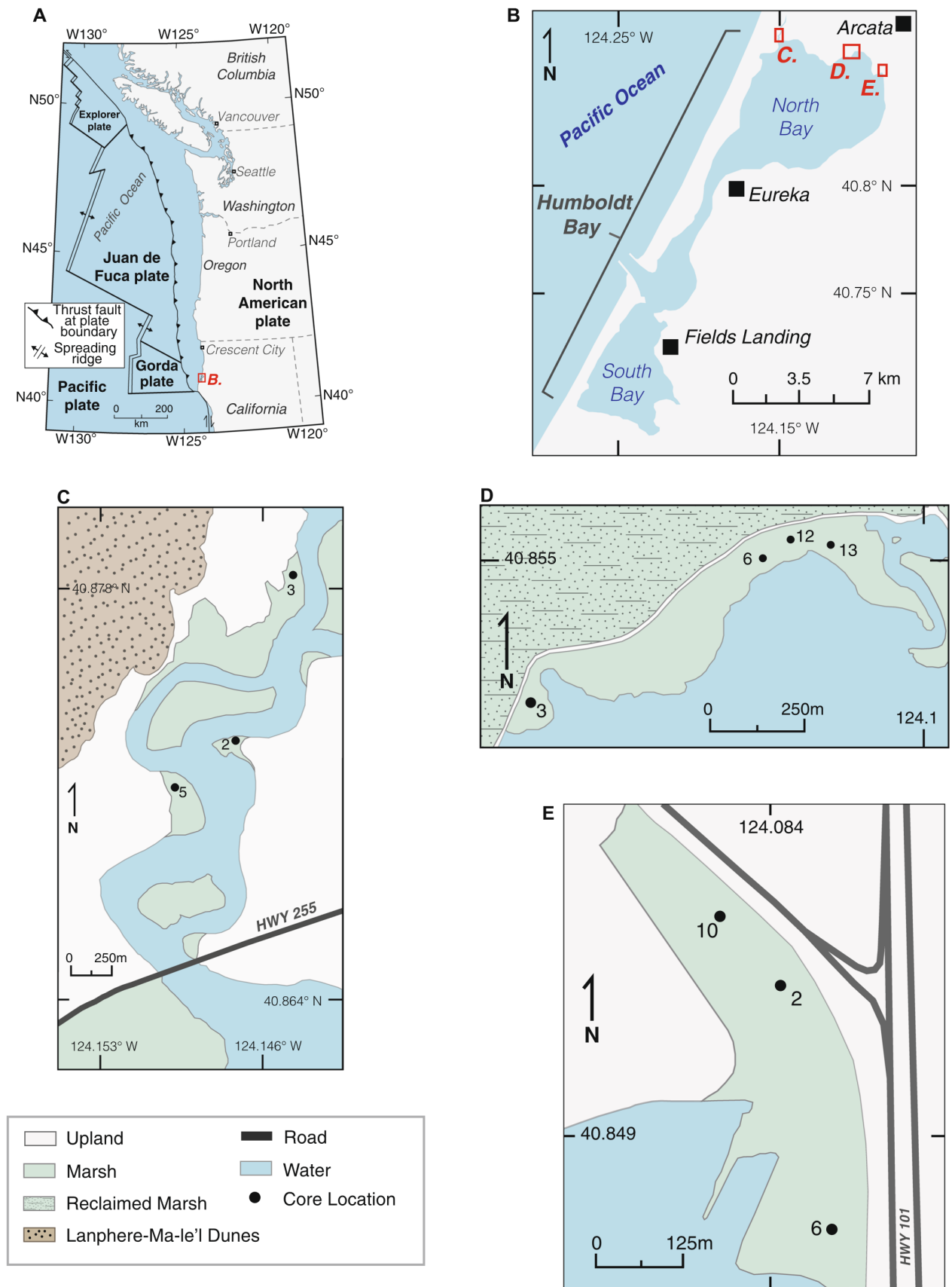
Figure 1. Location map of (A) Pacific Northwest of the United States and southwest Canada, (B) Humboldt Bay, (C) Mad River Slough, (D) McDaniel Creek, and (E) Jacoby Creek. [Color figure can be viewed at wileyonlinelibrary.com]

consistency of coseismic subsidence estimate distributions to identify within-site and within-bay stratigraphic and biostratigraphic variability.

Lithostratigraphic analysis

Stratigraphic description and sampling

Based on the stratigraphic mapping of Padgett *et al.* (2021) at northern Humboldt Bay, we selected a total of 20 representative stratigraphic sections (sediment cores) that span three earthquake-induced subsidence contacts from Mad River Slough (8), McDaniel Creek (7) and Jacoby Creek (5). Grain size, sedimentary structures, nature of contacts, unit thickness and facies changes were described in the field using general stratigraphic methods. Abrupt (1 mm), sharp (1–5 mm), clear (5–10 mm) and gradual (>10 mm) mud-over-peat contacts were mapped primarily using a 30 mm wide gouge core up to ~4 m below the ground surface. The tidal wetland stratigraphy consists of clastic mud and interbedded organic-rich units. A clastic 'mud' refers to a lithology of grey to olive-grey massive or finely (1–3 mm) bedded silts and clays. An 'organic-rich unit' refers to a light-to-dark brown salt-marsh peat. Sediment cores selected for chronological and biostratigraphic analyses were preferentially collected with an Eijkelkamp peat sampler.

Stratigraphic imaging

We followed several recent palaeoseismic studies to identify sediment core density contrasts (e.g. Goldfinger *et al.*, 2012; Briggs *et al.*, 2014; Witter *et al.*, 2019) and obtained high-resolution density imagery. The imagery guided lithostratigraphic analysis, i.e. identifying mixed interval lithologies, contact sharpness, continuity through the sediment core and informed interval selection for foraminiferal analysis above and below subsidence contacts. Computed tomography (CT) scans were conducted following the standard methodologies outlined by Rothwell and Rack (2006) and Davies *et al.* (2011) and were processed with a 'bone' algorithm to generate coronal images every millimetre across the core at Rhode Island South County Hospital and Oregon State University College of Veterinary Medicine. Where CT imagery was unavailable, we employed X-ray image analysis, which was conducted at the University of Rhode Island Health Center. Sediment core density images were joined into composite imagery and figures using Horos and Adobe Illustrator software.

Relative sea-level reconstructions

Foraminifera

We followed standard sample preparation and analysis (e.g. Scott and Medioli, 1980; de Rijk, 1995; Horton and Edwards, 2006). Foraminiferal samples were concentrated by sieving 1 cm thick intervals of sediment (~1–3 cm^3), from collected cores, over 500- and 63-micron sieves and retaining the material between those size fractions. The 500-micron sieve was checked for larger foraminifera before material was discarded. Foraminifera were identified following taxonomy based on Hawkes *et al.* (2010) and Milker *et al.* (2015). Additionally, we combined *Haplophragmoides* spp. and *Ammobaculites* spp. following Kemp *et al.* (2018). Foraminifera count numbers over 200 are likely to be overly conservative given the low diversity of salt-marsh foraminiferal assemblages (Kemp *et al.*, 2020). Following the results and recommendations of Kemp *et al.*, (2018, 2020),

we aimed to count 75–200 dead foraminifera per 1 cm sediment core interval or until the entire sample was enumerated.

Bayesian transfer function

Along the Cascadia coastal margin, foraminiferal-based transfer functions provide high-precision RSL reconstructions by statistically relating fossil assemblages to modern intertidal distributions (Guilbault *et al.*, 1995, 1996; Nelson *et al.*, 2008; Hawkes *et al.*, 2010, 2011; Engelhart *et al.*, 2013b; Wang *et al.*, 2013; Milker *et al.*, 2016; Kemp *et al.*, 2018). Typical Cascadia foraminiferal transfer functions have uncertainties of <±0.3–0.5 m (e.g. Guilbault *et al.*, 1995, 1996; Nelson *et al.*, 2008; Hawkes *et al.*, 2010, 2011; Engelhart *et al.*, 2013a, Wang *et al.*, 2013; Milker *et al.*, 2016; Kemp *et al.*, 2018; Nelson *et al.*, 2020; Padgett *et al.*, 2021). Within transfer functions, a standardised water-level index (SWLI) is used to relate samples taken from locations with different tidal ranges (Horton and Edwards, 2006). In 2018, Kemp *et al.* developed a foraminiferal BTF that builds on previous Cascadia transfer functions (e.g. Hawkes *et al.*, 2011; Milker *et al.*, 2016). The BTF of Kemp *et al.* (2018) incorporates a modern foraminiferal training set that spans from 32.5° to 50°N, allows for flexible species-elevation response curves, and can formally incorporate prior information from additional proxies, e.g. other microfossil groups, $\delta^{13}C$, or lithologic/stratigraphic context (Cahill *et al.*, 2016; Holden *et al.*, 2017). Based on these advantages, we employ the BTF of Kemp *et al.* (2018) in our variability assessment.

We assign informative priors based on lithologic/stratigraphic context following the approach of Kemp *et al.* (2018). A clastic dominated lithology likely formed as a tidal flat to low salt-marsh that accumulated at elevations between mean low water and MHHW (20–200 SWLI), even though clastic sediments can accumulate at elevations below 20 SWLI. An organic-rich-dominated lithology most likely formed as a high salt-marsh, which accumulates at elevations from MHW to the highest occurrence of foraminifera (180–252 SWLI; Kemp *et al.*, 2018). Errors are presented as one-sigma uncertainties to maintain consistency with previous results at Cascadia (e.g. Wang *et al.*, 2013; Kemp *et al.*, 2018). To evaluate goodness of fit between a fossil assemblage and a modern analogue, we used the Bray–Curtis distance metric (Kemp and Telford, 2015; Kemp *et al.*, 2018). Due to low species diversity, a threshold of less than the 20th percentile of the dissimilarity coefficient values is appropriate for salt-marsh foraminifera (Kemp and Telford, 2015).

To derive a subsidence estimate we use the distributions of the reconstructed RSL elevations from the first unmixed centimetre intervals above and below the subsidence contact. Where appropriate, we account for contact relief and avoid mixed lithologies based on visual appearance and density imagery. The density imagery was critical for lithologic assessments.

Consistency of subsidence estimates

Northern Humboldt Bay marshes may have experienced variable post-seismic sedimentation after past megathrust earthquakes. We anticipate that sites closer together should have experienced similar post-seismic sedimentation and, therefore, the BTF results should also reflect similar amounts of coseismic subsidence. Therefore, given that the BTF approach has been validated and shown to produce accurate coseismic subsidence estimates (Engelhart *et al.*, 2013a; Kemp *et al.*, 2018), if the BTF coseismic subsidence estimates diverge from each other, then that likely reflects inherent variability

across the estuary due to second-order processes. To potentially account for stratigraphic variability and decrease the possibility of a misrepresentation of coseismic subsidence, we compiled at least two RSL reconstructions per earthquake stratigraphic sequence at each of the three marsh locations.

We use the validated BTF approach to derive multiple coseismic subsidence estimates for the same earthquake stratigraphic sequence, and averaging the distributions, we reduce the associated error of subsidence estimates and highlight stratigraphic inconsistencies across a marsh and/or an estuary. For example, each RSL elevation estimate (stratigraphic interval) reconstructed by the BTF has a posterior distribution from which statistical summaries can be obtained and the associated uncertainty can be quantified. A 'subsidence estimate' is derived by taking the differences between N posterior samples of two reconstructed RSL elevations, which results in a subsidence distribution (Cahill et al., 2016; Kemp et al., 2018). An uncertainty reduction can result when subsidence samples are averaged from multiple sites because the average will be drawn to the region of greatest overlap in the individual subsidence distributions. We qualitatively assess the consistency of coseismic subsidence estimate distributions based on the overlap of probability density function distributions for the area/subsidence contact(s) in question and by performing a sensitivity analysis on the inclusion/exclusion of sites in the calculation of the intersite average estimates. By comparing proximate location estimates we gain insight into the extent of stratigraphic and biostratigraphic variability and build confidence in proposing an averaged representative estimate for the estuary. We use the Jensen–Shannon divergence (Menéndez

et al., 1997; Fuglede and Topsoe, 2004) to quantify the difference (or similarity) between subsidence distributions. This measure scores between 0 (identical) and 1 (maximally different).

RESULTS

Contact lithologies, foraminiferal assemblages and subsidence estimates

The tidal wetland stratigraphy throughout northern Humboldt Bay (Figs. 1 and 2) contains four organic-rich units overlain by mud units (Padgett et al., 2021). The organic-rich units contain relatively abundant plant macrofossils and, in general, the older and deeper buried organic-rich units are increasingly humified. Clastic mud units contained sparse plant macrofossils, are often massive, and occasionally finely bedded. We did not observe any sand layers in-between an organic-rich unit and overlying mud across the estuary.

For each marsh site and each subsidence contact (e.g. earthquakes 1, 2 and 3), we first describe the subsidence contact lithology observed in sediment cores and then the foraminiferal biostratigraphy (above and below subsidence contacts). Out of a total of 170 sample intervals (1 cm thick), we identified ≥200 fossil foraminifera in 132 intervals, 100–199 fossil foraminifera in 23 intervals and 40–99 fossil foraminifera in 15 intervals (Tables S1–S20). By applying the BTF to fossil foraminiferal assemblages above and below subsidence contacts, we derived quantitative coseismic
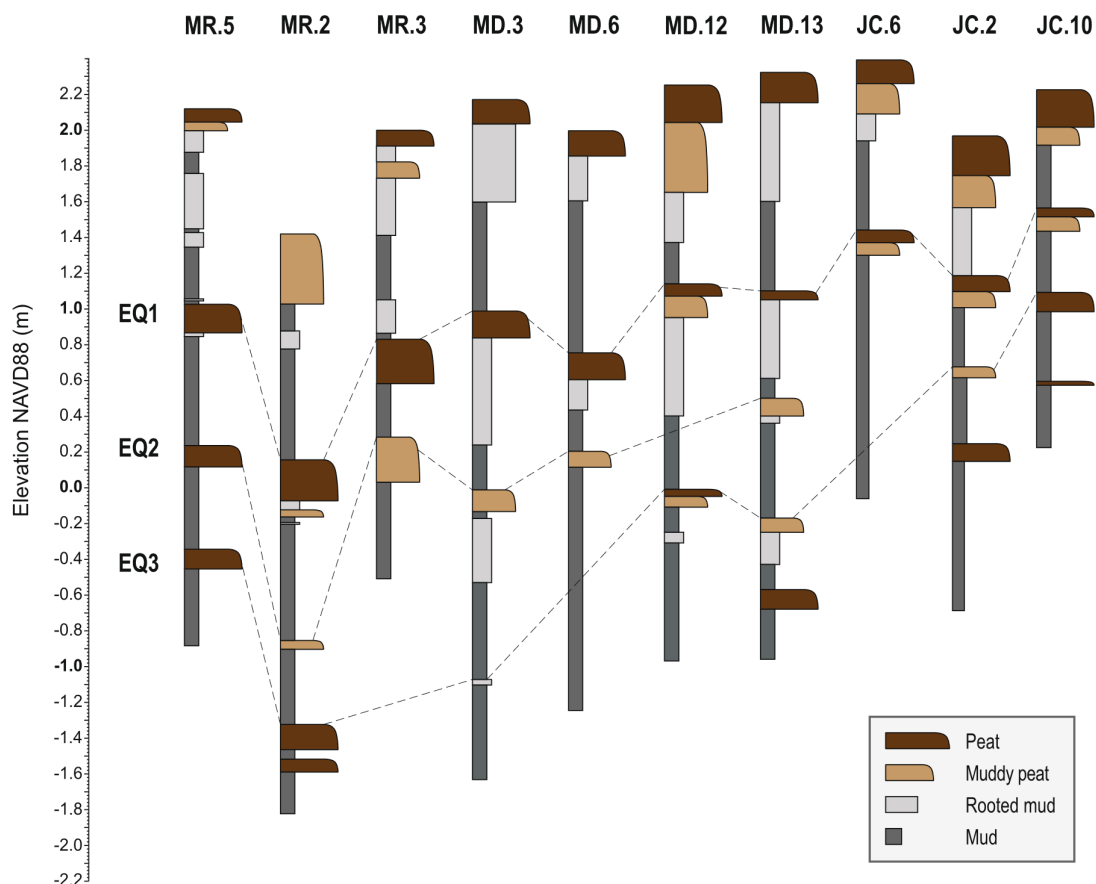

Figure 2. Simplified lithostratigraphy at northern Humboldt Bay based on the stratigraphy of Padgett et al., (2021) at Mad River Slough (MR), McDaniel Creek (MD) and Jacoby Creek (JC). [Color figure can be viewed at wileyonlinelibrary.com]

subsidence estimates and uncertainty (Table 1). Estimates are reported along with one-sigma uncertainties.

Earthquake 1 (1700 CE, 250 cal a BP)

At northern Humboldt Bay, the shallowest subsidence contact recorded in the tidal wetland stratigraphy has radiocarbon ages consistent with the most recent great earthquake at Cascadia in 1700 CE (250 cal a BP; Padgett *et al.*, 2021). The 1700 CE subsidence contact is the most prominent subsidence contact within the tidal wetland stratigraphic record (Padgett *et al.*, 2021). In total, we evaluated nine stratigraphic sections of the 1700 CE subsidence contact (Figs. 3–5) and three representative stratigraphic sections were collected from each marsh site for fossil foraminiferal analysis (Figs. 1, 3–5). The relief of the subsidence contact ranges from 3 to 19 mm (based on visual appearance and density imagery), which influences subsidence estimate derivations to be separated by up to 3 cm to avoid mixed lithology interval reconstructions (Table 1; Figs. 3–5; Tables S1–S9). The 1700 CE subsidence estimates show as much as 0.76 m of intersite variability (across the estuary) between JC.06 and MR.02 (Table 1; Figs. 4 and 5; Tables S1–S9).

McDaniel Creek

At *MD.03*, *MD.12* and *MD.13*, the three core sites display similar contact lithology and fossil foraminiferal biostratigraphy (Table 1; Fig. 3; Tables S1–S3). Foraminiferal assemblages within the organic-rich units dominantly consist of *Jadammina macrescens* (17–54%), *Trochammina inflata* (23–44%) and *Balticammina pseudomacrescens* (11–38%), which is consistent with a high salt-marsh peat environment, i.e. the BTF midpoint distributions of 212–200 SWLI. Although the fossil foraminifera assemblages within the mud units overlying the organic-rich units also contain *J. macrescens* (17–54%),

B. pseudomacrescens (1–29%) and *T. inflata* (16–44%), the assemblages also show a marked increase in the abundance of *Milliamina fusca* (≤21%), *Reophax* spp. (≤7%) and *Ammobaculites* spp. (≤5%), which is an assemblage that is consistent with sediments accumulating between MHW and mean tide level (MTL), i.e. BTF midpoint distributions of 169–125 SWLI. The subsidence estimates and uncertainty (±1 sigma) are 0.85 ± 0.46, 0.67 ± 0.48 and 0.84 ± 0.46 m, respectively, for *MD.03*, *MD.12* and *MD.13* (Table 1; Fig. 3; Tables S1–S3).

Jacoby Creek

At *JC.02*, *JC.06* and *JC.10*, sediment cores and density imagery display an abrupt-to-sharp undulatory subsidence contact (Table 1; Fig. 4; Tables S4–S6). Foraminiferal assemblages within the organic-rich unit dominantly consist of *B. pseudomacrescens* (20–58%), *T. inflata* (24–42%) and *J. macrescens* (14–41%), which is consistent with a high salt-marsh peat, and have BTF midpoint distributions of 210–197 SWLI. At *JC.02* and *JC.10*, even though assemblages in the grey mud units are also dominated by *J. macrescens* (39–67%), *T. inflata* (10–33%) and *B. pseudomacrescens* (3–24%), the assemblages show an increase in the abundance of *M. fusca* (1–30%), *Ammobaculites* spp. (≤8%) and *Reophax* spp. (≤7%), which are consistent with tidal environments accumulating between MHW and MTL, i.e. BTF midpoint distributions of 169–122 SWLI. At *JC.06*, foraminifera in the grey mud unit dominantly consist of *M. fusca* (45–52%), *T. inflata* (11–23%) and *J. macrescens* (16–23%) but also include *Ammobaculites* spp. (1–8%) and *Reophax* spp. (1–5%), which are typically associated with sediments accumulating below MHW. The relative abundance of *M. fusca* within the mud unit intervals used in the subsidence estimate derivation range from as little as 3% at *JC.02* to as much as 52% at *JC.06*, which influences the intrasite variability in the coseismic subsidence estimate

Table 1. Lithology and coseismic subsidence estimates from the northern Humboldt Bay estuary.

Core location	Contact depth (cm)	Nature of mud-over-peat contact*	Contact relief (mm)	Intervals skipped (cm)	SWLI below contact	SWLI above contact	Subsidence estimate ±1 standard deviation (m)	Intrasite average ±1 standard deviation (m)	Intersite average ±1 standard deviation (m)
Earthquake 1 – 250 cal a BP									
MD.03	115	a-s	4	2	203	130	0.85 ± 0.46	0.79 ± 0.28	0.64 ± 0.14
MD.12	109	a-s	6	0	206	155	0.67 ± 0.48		*0.81 ± 0.19#*
MD.13	121.5	a-s	17	2	200	128	0.84 ± 0.46		
JC.02	75.5	a	19	2	200	151	0.68 ± 0.52	0.84 ± 0.26	
JC.06	93.5	a	7	2	203	116	1.00 ± 0.44		
JC.10	79.5	s	11	2	199	128	0.83 ± 0.45		
MR.02	142	s	3	2	203	186	0.24 ± 0.27	0.29 ± 0.17	
MR.03	103	s-c	7	3	206	184	0.3 ± 0.3		
MR.05	105.5	s	16	3	209	183	0.33 ± 0.32		
Earthquake 2 – ca. 875 cal a BP									
MD.03	211	s	2	1	199	164	0.44 ± 0.35	0.43 ± 0.25	0.43 ± 0.16
MD.06	170.5	s	7	1	199	168	0.42 ± 0.37		
MR.02	220.5	s	2	0	197	159	0.41 ± 0.36	0.44 ± 0.22	
MR.03	149	s	3	0	195	165	0.42 ± 0.4		
MR.05	188	s	3	0	203	172	0.48 ± 0.39		
Earthquake 3 – ca. 1120 cal a BP									
MD.12	221	s	4	2	208	140	0.80 ± 0.49	0.79 ± 0.35	0.70 ± 0.18
MD.13	248	s	15	3	212	145	0.79 ± 0.47		
JC.02	131	s-c	12	1	202	151	0.70 ± 0.50	0.79 ± 0.33	
JC.10	124.5	s-c	3	2	205	129	0.88 ± 0.45		
MR.02	212	s-c	8	1	206	169	0.54 ± 0.43	0.50 ± 0.27	
MR.05	246	a	2	1	203	166	0.47 ± 0.36		

*Contacts: a-abrupt, 1 mm; s-sharp, 1-5 mm; c-clear, >5–10 mm; g-gradual, >10 mm. Number refers to number of observations.
#Intersite average without Mad River Slough subsidence estimates.
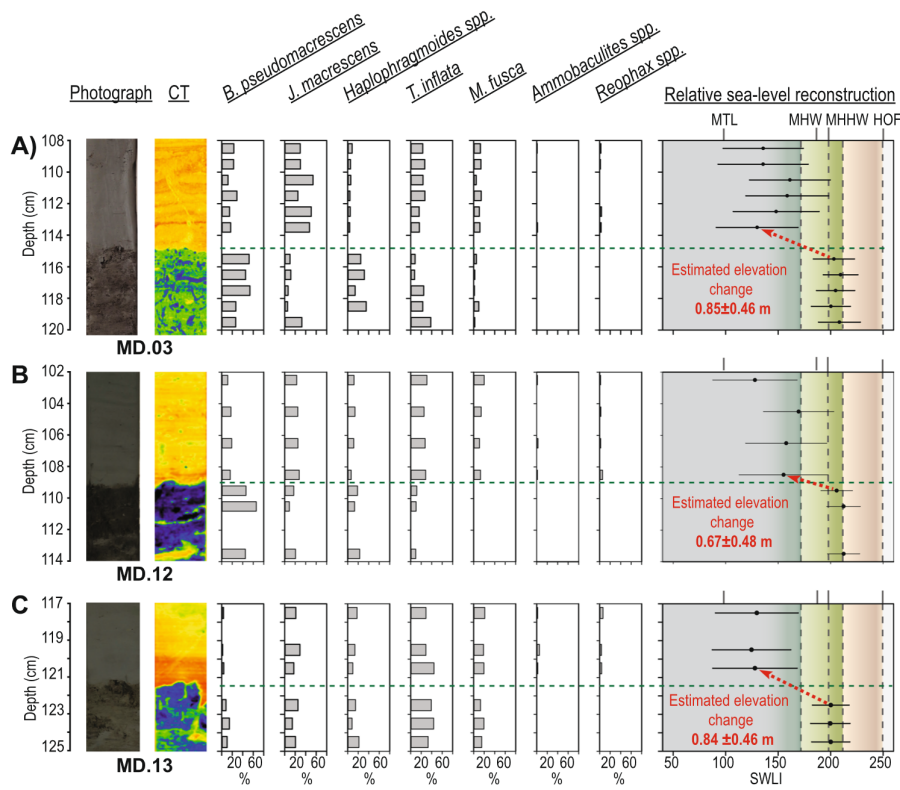SWLI: standardised water-level index.

Figure 3. Plots showing McDaniel Creek stratigraphy of the 1700 CE earthquake at three core sites: A. MD.03; B. MD.12; and C. MD.13. The plots include photo images, CT scans (rainbow scale; warm colours = more dense and cool colours = less dense), percentage foraminifera (grey bar) and results of BTF-reconstructed sea level with error bars that represent 1σ uncertainties. HOF: highest occurrence of foraminifera. SWLI: standardised water-level index. [Color figure can be viewed at wileyonlinelibrary.com]
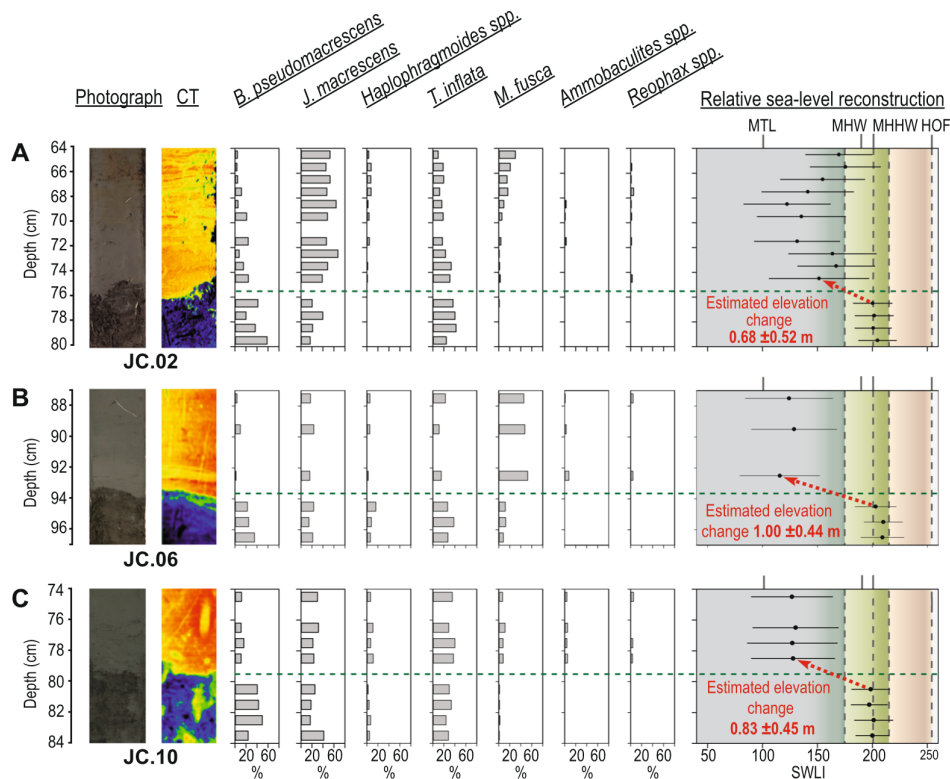

Figure 4. Plots showing Jacoby Creek stratigraphy of the 1700 CE earthquake at three core sites: A. JC.02; B. JC.06; and C. JC.10. The plots include photo images, CT scans (rainbow scale; warm colours = more dense and cool colours = less dense), percentage foraminifera (grey bar) and results of BTF-reconstructed sea level with error bars that represent 1σ uncertainties. HOF: highest occurrence of foraminifera. SWLI: standardised water-level index. [Color figure can be viewed at wileyonlinelibrary.com]
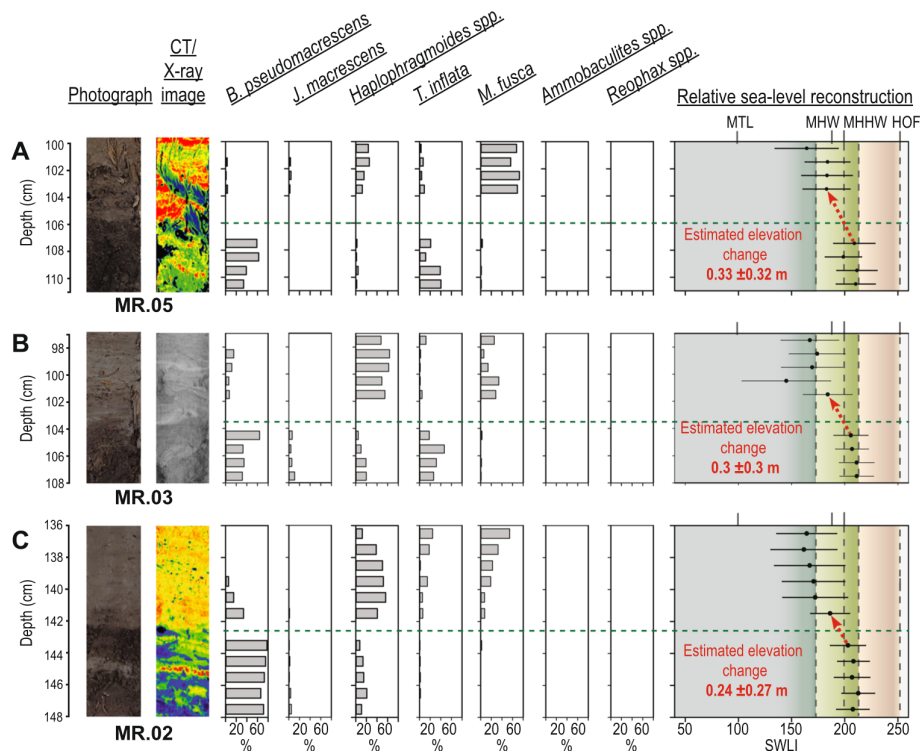
Figure 5. Plots showing Mad River Slough stratigraphy of the 1700 CE earthquake at three core sites: A. MR.05; B. MR.03; and C. MR.02. The plots include photo images, CT scans (rainbow scale; warm colours = more dense and cool colours = less dense), percentage foraminifera (grey bar) and results of BTF-reconstructed sea level with error bars that represent 1σ uncertainties. HOF: highest occurrence of foraminifera. SWLI: standardised water-level index. [Color figure can be viewed at wileyonlinelibrary.com]

distribution of 0.32 m. At *JC.02, JC.06* and *JC.10*, the subsidence estimates and uncertainty (±1 sigma) are 0.68 ± 0.52, 1.00 ± 0.44 and 0.83 ± 0.45 m, respectively (Table 1; Fig. 4; Tables S4–S6).

Mad River Slough

Even though *MR.05, MR.03* and *MR.02* span a ~800 m distance, the lithology, biostratigraphy and BTF subsidence estimate distributions are consistent (Table 1; Figs. 1 and 5; Tables S7–S9). The 1700 CE subsidence contact is sharp-to-clear and the density imagery shows sporadic organics within the mud units overlying the subsidence contacts (Fig. 5; Fig. S1). Additionally, at *MR.05* the photograph and CT image show a plant macrofossil, *Triglochin maritimum*, in growth position spanning the subsidence contact (Fig. 5A). Within the organic-rich units, foraminifera assemblages are dominated by *B. pseudomacrescens* (32–62%), *Haplophragmoides* spp. (11–40%) and *T. inflata* (15–22%), which is consistent with a high salt-marsh peat environment, and have BTF midpoint distributions that range between 213 and 199 SWLI. Foraminiferal assemblages within the mud units are dominated by *M. fusca* (7–73%) and *J. macrescens* (12–64%), which is consistent with environments forming below MHW, i.e. BTF distributions of 162–186 SWLI. At *MR.03* and *MR.05* the assemblages from the mud unit intervals used in the subsidence derivation also contain several *Milliamina petila*, which are typically found above MHHW (Fig. 5 and Tables S7–S9). However, the mud unit BTF results did not exceed the 20th percentile threshold dissimilarity coefficient, i.e. have modern analogues. The subsidence estimates suggest 0.33 ± 0.32, 0.3 ± 0.3 and 0.24 ± 0.27 m of subsidence at *MR.05, MR.03* and *MR.02*, respectively (Table 1; Fig. 5; Tables S7–S9).

Earthquake 2 (ca. 875 cal a BP)

Radiocarbon analysis and Bayesian age modelling results suggest that the second most recent subsidence contact observed within the tidal wetland stratigraphic record at northern Humboldt Bay occurred ca. 875 cal a BP (Padgett *et al.*, 2021). However, a subsidence contact for earthquake 2 was not observed at Jacoby Creek (Padgett *et al.*, 2021); direct evidence that subsidence stratigraphy is not always continuous across all sites within an estuary. In total, we evaluated five stratigraphic sections: two from McDaniel Creek and three from Mad River Slough (Figs. 6 and 7). The ca. 875 cal a BP earthquake subsidence contact was observed at depths between 149 and 220.5 cm below the modern marsh surface with thicknesses that range from 3 to 4 mm (Table 1; Fig. S2). The relief of the contacts range from 2 to 7 mm, which limited the intervals avoided in the derivation of subsidence estimates to ≤1 cm (Figs. 6, 7; Table 1; Fig. S2). Even though the sediment cores were collected over a ~3500 m distance, the BTF subsidence estimate midpoint distributions suggest 0.07 m of intersite variability (Table 1; Figs. 1, 6 and 7).

McDaniel Creek

At *MD.06* and *MD.03*, a sharp-to-clear contact separates an organic-rich unit from an overlying mud unit at 170.5 and 211 cm core depths, respectively (Fig. 6). At *MD.03*, the mud unit overlying the contact contains very thin (1–3 mm) laminations in the lower 10 cm of the unit (Figs. 6 and S2). Foraminiferal assemblages within the organic-rich units dominantly consist of *B. pseudomacrescens* (12–40%), *J. macrescens* (14–30%) and *T. inflata* (24–36%), which is consistent with high salt-marsh peat environments, i.e. BTF midpoint distributions of 199–207 SWLI (Fig. 6; Tables S10–S11).
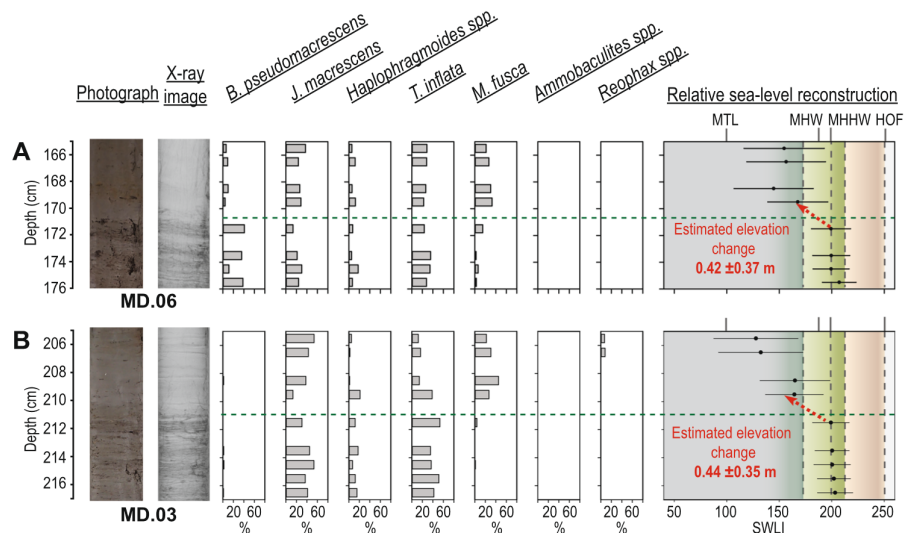
Figure 6. Plots showing McDaniel Creek stratigraphy of the ca. 875 cal a ʙᴘ earthquake at two core sites: A. MD.14.06; and B. MD.14.03. The plots include photo images, CT scans (rainbow scale; warm colours = more dense and cool colours = less dense), percentage foraminifera (grey bar) and results of BTF-reconstructed sea level with error bars that represent 1σ uncertainties. HOF: highest occurrence of foraminifera. SWLI: standardised water-level index. [Color figure can be viewed at wileyonlinelibrary.com]
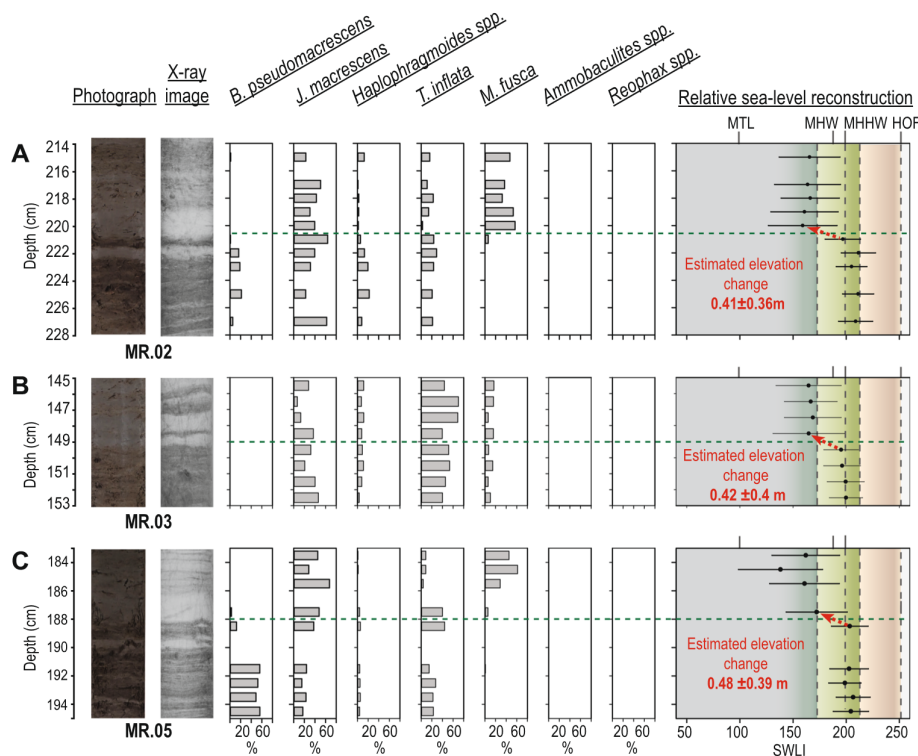

Figure 7. Plots showing Mad River Slough stratigraphy of the ca. 875 cal a ʙᴘ earthquake at three core sites: A. MR.02; B. MR.03; and C. MR.05. The plots include photo images, CT scans (rainbow scale; warm colours = more dense and cool colours = less dense), percentage foraminifera (grey bar) and results of BTF-reconstructed sea level with error bars that represent 1σ uncertainties. HOF: highest occurrence of foraminifera. SWLI: standardised water-index. [Color figure can be viewed at wileyonlinelibrary.com]

Foraminiferal assemblages within the mud units show an increase in the abundance of *M. fusca* (21–33%) which is consistent with sediments accumulating below MHW and have BTF midpoint distributions of 128–167 SWLI. The foraminiferal assemblages within the mud unit intervals used in the subsidence derivation at *MD.03* and *MD.06* (i.e. the first mud unit intervals above the subsidence contact) both contain *T. inflata* (40% and 24%) and *J. macrescens* (28% and 13%) and have similar BTF midpoint distributions of 164 and 167 SWLI (Tables S10–S11; Fig. S2), which produces similar subsidence estimate distributions of 0.44 ± 0.35 m and 0.42 ± 0.37 m, respectively (Table 1; Fig. 6; Tables S10–S11).

Mad River Slough

At *MR.02*, *MR.03* and *MR.05*, the photographs and density imagery show a sharp-to-clear horizontal contact throughout the marsh site (Figs. 7 and S2). However, the stratigraphy above and below the subsidence contacts differs from typical subsidence stratigraphy. For example, below the subsidence contact at *MR.02* and *MR.05*, there is a ~1 cm thick mud lens 5–8 mm below the upper contact of the peat units. Additionally, at *MR.03*, the mud becomes rooted ~2 cm above the subsidence contact. However, foraminiferal assemblages do not differ within either the mud lens or within the rooted intervals compared with the assemblages above and below. Despite the less than typical subsidence stratigraphy, we found little intrasite subsidence estimate variability; BTF subsidence estimate midpoint distributions differ by 0.07 m (Table 1; Fig. 7).

The consistency of subsidence estimates can be attributed to the foraminiferal assemblages (Fig. 7; Tables S12–14). At *MR.03*, foraminiferal assemblages above and below the subsidence contact are very similar (Fig. 7; Table 13). Within the organic-rich unit, foraminifera assemblages dominantly consist of, but also contain, *M. fusca* (6–17%) and within the overlying rooted mud the assemblages also contain *T. inflata* (39–70%), *J. macrescens* (23–50%) and *M. fusca* (6–15%). Additionally, even though *MR.02* and *MR.05* are separated by the main channel of Mad River Slough, the foraminiferal assemblages above and below the contact are generally very similar. For example, within the mud units, foraminiferal assemblages are dominated by *J. macrescens* (23–67%) and *M. fusca* (6–61%), which is consistent with sediment accumulating below MHW, i.e. BTF midpoint distributions that range between 138 and 172 SWLI. The relative percentages of *M. fusca* (6–61%), within the interval used in the subsidence estimate derivation drive the differences between the subsidence estimates. The subsidence estimates are 0.48 ± 0.39, 0.42 ± 0.4 and 0.41 ± 0.36 m at *MR.02*, *MR.03* and *MR.05*, respectively (Table 1; Fig. 7; Tables S12–S14).

Earthquake 3 (ca. 1120 cal a BP)

Stratigraphic mapping, radiocarbon ages of plant macrofossils and Bayesian age modelling suggest that the third shallowest submergence occurred ca. 1120 cal a BP (Padgett *et al.*, 2021).

We selected six stratigraphic sections for foraminiferal analysis that contain the earthquake 3 contact; two from each marsh site (Figs. 1, 8–10 and S3). Photographs and density imagery of fossil sediment cores reveal an abrupt-to-clear contact with relief that ranges from 2 to 15 mm (Table 1; Figs. 8–10 and S3). We avoid mixed lithologies within subsidence estimate derivations by selecting intervals spanning 1–3 cm across the submergence contact (Table 1; Figs. 8–10). Subsidence estimate distributions suggest as much as 0.17 m of intrasite variability and 0.41 m of intersite variability (Table 1).

McDaniel Creek

At *MD.12* and *MD.13*, the BTF midpoint distribution results provide nearly identical subsidence estimates (Table 1; Fig. 8). Despite CT imagery showing a burrow that vertically infiltrates ~3–4 cm down into the organic-rich unit at *MD.12*, the biostratigraphy is very similar at *MD.12* and *MD.13* (Figs. 9 and S3; Tables S15–16). Foraminiferal assemblages within the organic-rich units dominantly consist of *Haplophragmoides* spp. (11–67%), *B. pseudomacrescens* (3–62%), *T. inflata* (9–71%) and *J. macrescens* (22–52%), which is consistent with high salt-marsh peat environments, e.g. BTF midpoint distributions of 198–211 SWLI. Foraminifera assemblages in the mud units dominantly consist of *M. fusca* (14–19%) and *J. macrescens* (13–54%) but also contain *Reophax* spp. (1–9%) and *Ammobaculites* spp. (1–10%), which is consistent with sediments accumulating between MTL and MHW, i.e. BTF midpoint distributions of 117–145 SWLI. The subsidence estimates are 0.80 ± 0.49 at *MD.12* and 0.79 ± 0.47 at *MD.13* (Table 1; Fig. 8).

Jacoby Creek

At *JC.02* and *JC.10* the earthquake 3 subsidence contact is sharp-to-clear and undulatory (Table 1; Figs. 9 and S3). Foraminiferal assemblages show high consistency within the organic-rich units and consist of *B. pseudomacrescens* (48–69%), *T. inflata* (15–27%) and *J. macrescens* (6–24%), which is consistent with a high salt-marsh peat, i.e. BTF midpoint distributions range from 202 to 205 SWLI. However, the foraminiferal assemblages within the
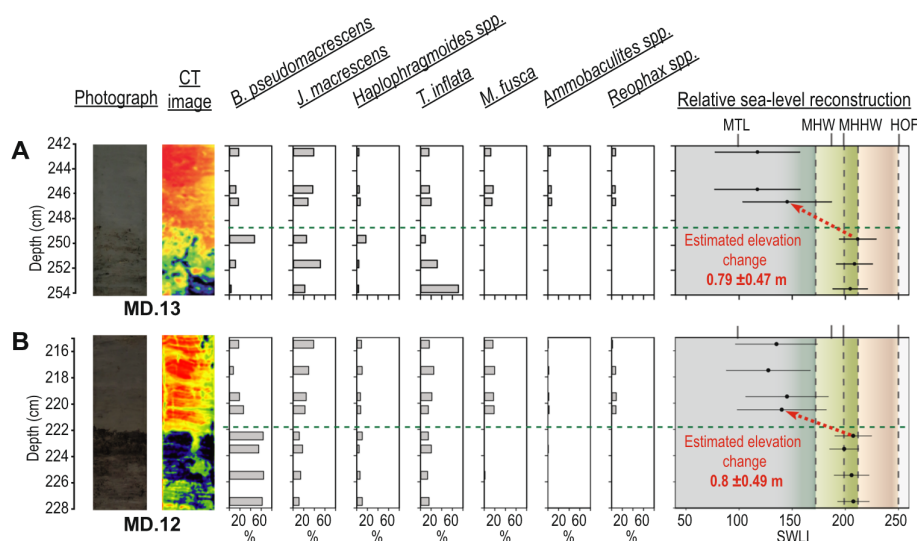

Figure 8. Plots showing Jacoby Creek stratigraphy of the ca. 1120 cal a BP earthquake at two core sites: A. JC.02; and B. JC.10. The plots include photo images, CT scans (rainbow scale; warm colours = more dense and cool colours = less dense), percentage foraminifera (grey bar) and results of BTF-reconstructed sea level with error bars that represent 1σ uncertainties. HOF: highest occurrence of foraminifera. SWLI: standardised water-level index. [Color figure can be viewed at wileyonlinelibrary.com]
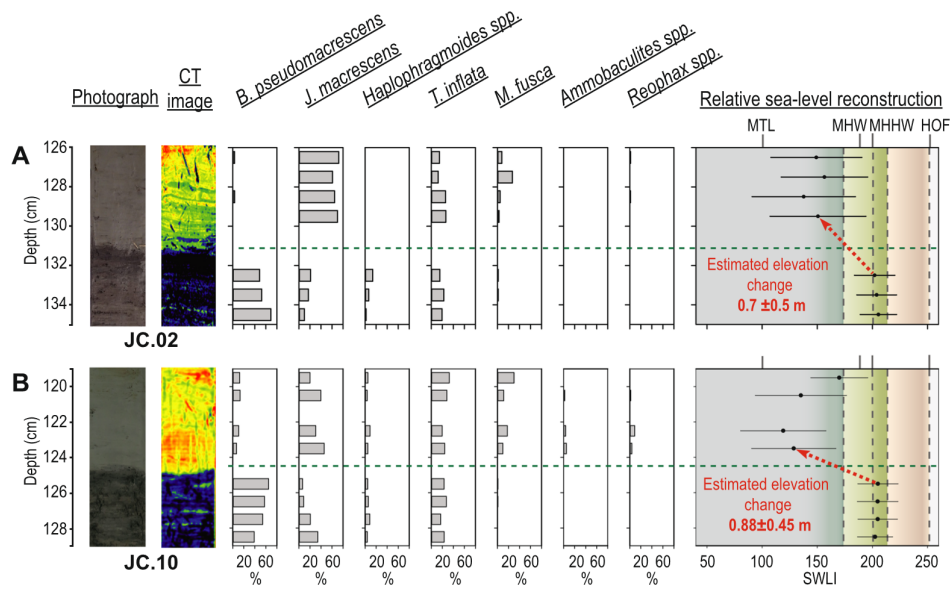
Figure 9. Plots showing McDaniel Creek stratigraphy of the ca. 1120 cal a BP earthquake at two core sites: A. MD.13; and B. MD.12. The plots include photo images, CT scans (rainbow scale; warm colours = more dense and cool colours = less dense), percentage foraminifera (grey bar) and results of BTF-reconstructed sea level with error bars that represent 1σ uncertainties. HOF: highest occurrence of foraminifera. SWLI: standardised water-level index. [Color figure can be viewed at wileyonlinelibrary.com]

Figure 10. Plots showing Mad River Slough stratigraphy of the ca. 1120 cal a BP earthquake at three core sites: A. MR.14.05; B. MR.14.02. The plots include photo images, CT scans (rainbow scale; warm colours = more dense and cool colours = less dense), percentage foraminifera (grey bar) and results of BTF reconstructed sea level with error bars that represent 1σ uncertainties. HOF: highest occurrence of foraminifera. SWLI: standardised water-level index. [Color figure can be viewed at wileyonlinelibrary.com]
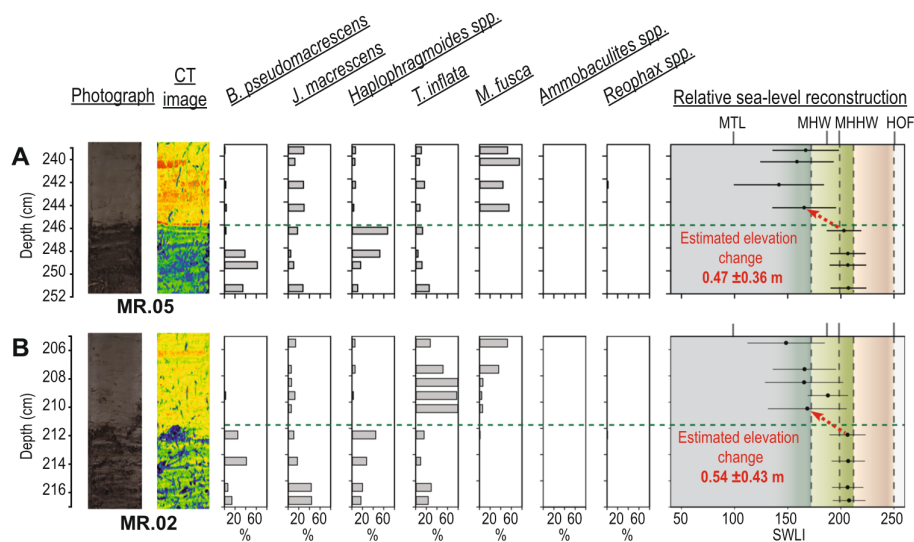
overlying mud units are less uniform and have BTF midpoint distributions that range from 119 to 170 SWLI (Tables S17–S18; Fig. 9). Foraminiferal assemblages in the overlying mud unit dominantly consist of *J. macrescens* (30–46%), *T. inflata* (20–33%) and *M. fusca* (10–30%), which is consistent with sediments accumulating below MHHW. The intervals directly overlying the subsidence contacts at *JC.02* and *JC.10* have BTF midpoint distributions at 151 SWLI and 129 SWLI, respectively. The differing post-seismic intertidal environments are partially due to the presence of *Reophax* spp. and *Ammobaculites* spp., which were only observed within the *JC.10* fossil sediment core (Tables S17–S18; Fig. 9). The subsidence estimates are 0.70 ± 0.50 m and 0.88 ± 0.45 m, respectively, for *JC.02* and *JC.10* (Table 1; Fig. 9).

Mad River Slough

At *MR.02* and *MR.05*, the earthquake 3 subsidence contact is horizontal and abrupt-to-clear (Table 1; Figs. 10 and S3). Foraminifera assemblages in the organic-rich units are consistent across the marsh and dominated by *Haplophrag-moides* spp. (11–67%), *J. macrescens* (5–44%) and *B. pseudomacrescens* (3–62%), which is consistent with a high salt-marsh peat, e.g. BTF midpoint distributions at 203–208 SWLI (Tables 1, S19–S20). Although foraminiferal assemblages within the mud units reflect more variability across the marsh, they are still consistent with sediments accumulating between MTL and MHW and have BTF midpoint distributions that range from 142 to 188 SWLI. For example, at *MR.02* foraminiferal assemblages are dominated by *T. inflata*
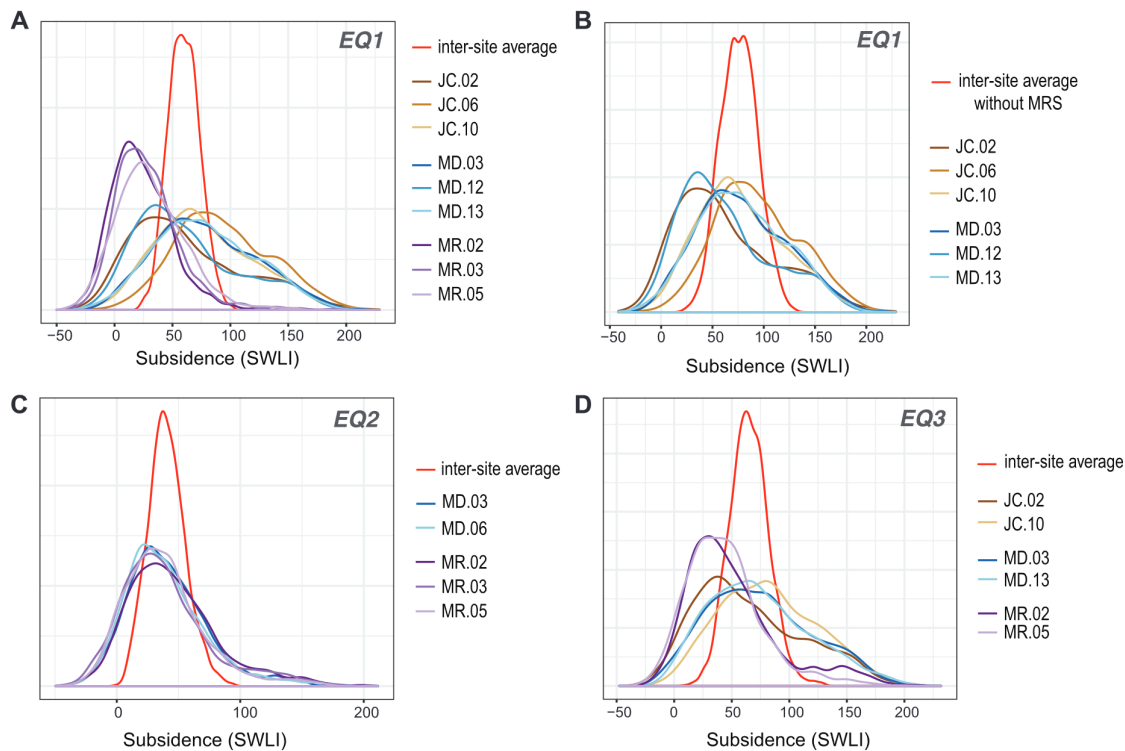
Figure 11. A. Graph of nine coseismic subsidence estimate BTF probability density functions and the averaged distribution, for the 1700 CE earthquake; B. graph of six coseismic subsidence estimate BTF probability density functions (Mad River Slough (MR) site removed) and the averaged distribution, for the 1700 CE earthquake; C. graph of five coseismic subsidence estimate BTF probability density functions and the averaged distribution, for the ca. 875 cal a BP earthquake; D. graph of five coseismic subsidence estimate BTF probability density functions and the averaged distribution, for the ca. 1120 cal a BP earthquake. [Color figure can be viewed at wileyonlinelibrary.com]

(27–88%) but at *MR.05* assemblages are dominated by *M. fusca* (44–75%) and *J. macrescens* (13–30%). However, the intervals used in the subsidence estimate derivations have BTF midpoint distributions of 169 SWLI at *MR.02* and 166 SWLI at *MR.05*. The subsidence estimates for *MR.02* and *MR.05* are, respectively, 0.54 ± 0.43 and 0.47 ± 0.36 m (Table 1; Fig. 10).

Intra- and intersite coseismic subsidence estimate variability

The subsidence estimates for each earthquake contact display limited intrasite variability. Intrasite variability of coseismic subsidence estimates (midpoint to midpoint) ranges from a maximum of 0.32 m for the 1700 CE earthquake at Jacoby Creek to a minimum of 0.01 m for the 1120 cal a BP earthquake at McDaniel Creek (Table 1; Fig. 11). If the RSL reconstructions were not repeated and averaged across the same stratigraphic sequence, then a single subsidence estimate could potentially be either an over- or under-representation of coseismic subsidence. However, each coseismic subsidence estimate distribution falls within the one-sigma range of the intrasite averaged estimate distribution (Table 1; Fig. 11), which supports reliability of the foraminiferal BTF approach (Kemp *et al.*, 2018).

Across three marsh sites, we observed intersite variability in the subsidence estimates for each earthquake contact (Table 1; Figs. 3–11). For site-averaged subsidence estimates, per earthquake contact, intersite variability ranged from a maximum of 0.55 m for the 1700 CE subsidence contact, to a minimum of 0.01 m for the ca. 1120 cal a BP subsidence contact (Table 1). For individual core locations, intersite subsidence estimate distribution variability ranges from a maximum of 0.76 m between *JC.06* (1.00 ± 0.44 m) and *MR.02* (0.24 ± 0.27 m) for

the 1700 CE earthquake, to a minimum of 0.00 m between *MD.06* (0.42 ± 0.37 m) to *MR.03* (0.42 ± 0.34 m) for the ca. 875 cal a BP earthquake (Table 1; Figs. 3–11). Excluding subsidence estimates for the 1700 CE earthquake at Mad River (cores *MR.02* and *MR.03*), each individual coseismic subsidence estimate range overlaps with the averaged intersite coseismic subsidence estimate.

DISCUSSION

Our results suggest that for the same earthquake stratigraphic sequence there is variability in foraminiferal assemblages and accompanying coseismic subsidence estimates both within a single marsh and across multiple marshes in an estuary. This variability generally falls within the one-sigma uncertainty but in limited cases falls outside of these constraints. These findings solicit several questions. What explains intra- and intersite variability of foraminiferal-based coseismic subsidence estimates? What is the appropriate geospatial extent to use in the determination of a coseismic subsidence estimate? How many sites, and for each site, how many fossil assemblage analyses per subsidence contact are needed to provide consistency of coseismic subsidence estimates? Whilst we have used examples from the CSZ, these questions and their answers are broadly relevant at subduction zones globally where transfer functions have or could be applied, such as the Hikurangi margin (New Zealand), the Alaska–Aleutian subduction zone (USA) or along the active margins of Japan.

On small vertical scales, lithostratigraphic (e.g. 0.1–10 mm) and biostratigraphic (e.g. 1–10 cm) observations provide insight into how second-order processes may impact microfossil-based subsidence estimates. As noted in the introduction, there are

several potential second-order factors that may influence fossil foraminifera-based BTF subsidence estimates. In most cases if the sediment core collection site is carefully selected with potential complications in mind, factors such as erosion and compaction can be *a priori* avoided, whereas other variables may not be evident until fossil sediment cores undergo lab analysis, e.g. microfossil and density imagery analysis. Therefore, we distinguish more likely concerns from other concerns that can likely be avoided by careful field descriptions and sampling. Using our lithostratigraphic and biostratigraphic datasets as reference, we discuss factors that could introduce variability into foraminiferal-based BTF subsidence estimates at different scales, including within a specific sediment core, at a marsh site and across an estuary.

We find that intrasite variability is primarily driven by foraminiferal assemblages within the mud units overlying the subsidence contact. Because second-order processes can influence such variability, identifying their impact on stratigraphic and biostratigraphic records is integral to deriving a representative subsidence estimate for a marsh and/or across an estuary. Our dataset allows us to highlight instances of mixing that contribute to intra- and intersite variability of coseismic subsidence estimates (i.e. 1700 CE at Mad River Slough). Even though there is lithostratigraphic and biostratigraphic variability, the data suggest that coseismic subsidence estimates derived from foraminiferal transfer functions are not only reproducible from closely spaced cores (<~45–100 m) but that estimates can also be reproduced 100's to 1000's of metres apart and across multiple marshes within an estuary (1–6 km apart). Our findings are also consistent with coastal palaeoseismic transfer function investigations utilising diatoms at other subduction zones (e.g. Shennan and Hamilton, 2006; Shennan et al., 2014). Therefore, we conclude that multiple spread-out replications of foraminiferal-based coseismic subsidence estimates should be used to provide increased confidence in the results.

Foraminiferal assemblages that may impact coseismic subsidence estimate variability

Mixed foraminiferal assemblages below a subsidence contact

Several Cascadia foraminiferal-based palaeogeodetic investigations have observed evidence of overlying mud infiltration into the pore space of underlying organic-rich units (e.g. Nelson et al., 1996b; Engelhart et al., 2013a; Milker et al., 2016) and that may influence subsidence estimates. At Osprey Marsh (Coquille River, Oregon) for the CSZ 1700 CE subsidence contact, Engelhart et al. (2013a) infer sediment infiltration from the presence of the low-marsh foraminifer M. fusca at high percentages within an organic-rich unit that is inferred to be the AO horizon of a forest soil ≥3 cm below the subsidence contact. Similarly, Milker et al. (2016) report mud infiltration 2 cm below two subsidence contacts at Talbot Creek, Oregon, based on the high percentages of M. fusca within organic-rich units. Downward mixing may be limited by the presence of a tsunami-sand (Kemp et al., 2018) but no tsunami-sand was observed at our sites. However, Kemp et al. (2018) show that mixed foraminiferal assemblages (e.g. presence of M. fusca at the top of the peat) found below a subsidence contact from a marsh transplant experiment (Engelhart et al., 2013a) can be accounted for by using informative constraints with the BTF. Herein, we follow Kemp et al., (2018) and Padgett et al. (2021), and assign lithologic informative constraints in our BTF analysis. Assigning informative lithologic constraints minimises the effect of mud infiltration that leads to mixed fossil assemblages below subsidence contacts.

However, downward mixing and the use of informative priors cannot fully account for the coseismic subsidence estimate

variability observed at northern Humboldt Bay because we did not observe mixed fossil assemblages within the organic-rich units that underlie the subsidence contacts. In fact, our biostratigraphic results indicate that all organic-rich unit intervals contain foraminiferal assemblages consistent with a high-marsh peat environment that formed at elevations near to or above MHHW. The estuary-wide BTF results indicate the organic-rich units have midpoint distributions that range from 195 to 213 SWLI, which is only a 20 cm (2.26–2.46 m NAVD88) variation across the estuary and an average of ~6.6 cm of variation per each organic-rich unit. Therefore, there is no evidence of mixing below subsidence contacts that can explain the subsidence variability observed within the individual marsh sites and throughout the estuary.

Mixed foraminiferal assemblages above a subsidence contact

Several wetland stratigraphic investigations have reported instances of fossil foraminiferal assemblage mixing within lower intertidal facies (e.g. Figueira and Hayward, 2014; Milker et al., 2016). The potential for mixing and reworking at lower tidal elevations is likely to be enhanced by the absence of vegetation that serves to stabilise sediments and reduce mobility (Allen, 2000). On the South Island of New Zealand, at Waikawa Harbor salt marsh, Figueira and Hayward (2014) document mixed faunas at modern low-tidal environments and conclude that localised marsh bank failure, possibly during a storm, reworked high-marsh species into the lower tidal elevations. Milker et al. (2016) also found high-marsh species in higher than expected proportions within the mud units that overlie the 1700 CE contact at Talbot Creek, Oregon. Milker et al. (2016) attributed the presence of the higher-marsh species, B. pseudomacrescens, in the mud unit to the brackish conditions of Talbot Creek locality, which is >6 km upstream from Coos Bay estuary, and inferred that the derived estimate of coseismic subsidence is probably a minimum estimate.

At northern Humboldt Bay, foraminiferal assemblages found within mud units that overlie subsidence contacts are the primary driver of the magnitude of subsidence estimates. Percentages of M. fusca, Reophax spp. and Ammobaculites spp. are common in mud units because these species' optimal elevations are below MHW, where minerogenic sediments dominate the depositional environment (Guilbault et al., 1995, 1996; Nelson et al., 1996b; Shennan et al., 1996; Hawkes et al., 2010, 2011; Engelhart et al., 2013a, b; Wang et al., 2013; Milker et al., 2015, 2016; Kemp et al., 2018). However, the composition of foraminiferal assemblages, especially the relative abundances of species with optimal elevations below MHW, found within mud units that overlie a subsidence contact is not always consistent within a marsh and/or across an estuary. Specifically, the estuary-wide BTF results indicate that the mud units contain foraminiferal assemblages consistent with environments that formed within a broad elevation range, roughly between MHW and MTL, i.e. BTF midpoint distributions that range from 116 to 188 SWLI (1.42–2.19 m NAVD88). Analysis of foraminiferal species compositions within mud units that overlie subsidence contacts can help document the extent of post-seismic biostratigraphic and depositional variability.

Throughout Mad River Slough, we observed low-marsh species and high-marsh species within the mud units overlying the 1700 CE subsidence contact, which contribute to lower coseismic subsidence estimates and a lower intrasite variability range (Table 1). For example, at MR.05, the foraminiferal assemblages are dominated by M. fusca but also contain M. petila (Fig. S2); two species that have elevation optima that do not overlap (Kemp et al., 2018). Even though the assemblages

did not exceed the modern analogue threshold limit, the occurrence of a relatively high percentage of *M. fusca* and the presence of *M. petila* are unlikely (Kemp *et al.*, 2018) and suggest a strong possibility of a mixed assemblage. The finding of a mixed assemblage that does not exceed the modern analogue threshold limit highlights the challenges of identifying non-analogue and analogue situations (Kemp and Telford, 2015). The presence of mixed assemblages can be the result of second-order processes, which can contaminate the derivation of coseismic subsidence estimates and potentially influence the relative consistency measures both at a site and across an estuary.

Mixed assemblages above the 1700 CE subsidence contact at Mad River Slough requires consideration of second-order processes influencing post-seismic deposition. The density imagery shows that the mud units overlying the 1700 CE contacts at Mad River Slough contain sporadic organics and irregular bedding planes (Figs. 3–5), which are quite different from the massive and finely laminated mud units at Jacoby Creek and McDaniel Creek (Figs S1–S8). A possible explanation is that Mad River Slough is a different intertidal environmental setting from the other marsh sites. Jacoby Creek and McDaniel Creek marshes are located at the mouths of small mountainous creeks that have year-round continuous discharge and empty into open-bay environments. In contrast, the Mad River Slough watershed lacks a high-relief headwater landscape; the slough is simply the downstream end of an overflow channel that, at the upstream end, connects to the Mad River. The slough accommodates infrequent flood overflow when Mad River levees are overtopped. The slough is confined on the west by the coastal Lanphere Dunes sequence, and on the east by a low divide separating west-flowing low-gradient drainage into the slough from northerly flowing low-gradient drainage into the Mad River. Therefore, the Mad River Slough watershed is smaller, less steep and experiences less discharge than McDaniel Creek and Jacoby Creek. Moreover, Mad River Slough has a more restricted access to the open-bay source, i.e. lower tidal-flux velocities, than the other two marsh sites (Fig. 1). Therefore, the lithostratigraphic and biostratigraphic characteristics observed above the 1700 CE subsidence contact at Mad River Slough may be explained by the local surface hydrology and physiographic position within the estuary.

Consequently, based on mixed fauna compositions, a differing environmental setting and density imagery, we infer that the lower section of the mud units overlying the 1700 CE contact at Mad River Slough are not representative of processes that occurred throughout northern Humboldt Bay estuary. The variability between the 1700 CE contact at Mad River Slough and the sites at Jacoby Creek and McDaniel Creek can be demonstrated in sensitivity analyses on the inclusion/exclusion of sites for the intersite averaged estimates (Fig. S4). The results show a divergence between sites for 1700 CE estimates with a maximum Jensen–Shannon divergence of 0.53 between *MR.02* and *JC.06*. Subsequent removal of the Mad River Slough estimates from the 1700 CE estuary-wide average calculation changes the average subsidence estimate from 0.64 ± 0.14 m to 0.81 ± 0.19 m, which is consistent within error of previous microfossil-based subsidence estimates (Pritchard, 2004; Engelhart *et al.*, 2016; Padgett *et al.*, 2021). Therefore, because we can account for the variability introduced by highly localised processes that are not present at the other two marsh sites, we do not use the Mad River Slough 1700 CE estimates in our estimate of estuary-wide average coseismic subsidence.

We note that the subsidence estimate variability between Mad River Slough and McDaniel Creek/Jacoby Creek is not observed for the ca. 875 cal a BP earthquake (Jensen–Shannon

divergence ranges from 0 to 0.01) and is reduced for the ca. 1120 cal a BP earthquake (Jensen–Shannon divergence ranges from 0 to 0.17; Fig. S4). Whilst we cannot provide a definitive answer to why this might be, one possibility could be that the geomorphic setting of Mad River Slough is temporally variable. Considering the disparity, estimates are provided both with and without Mad River Slough for the 1700 CE earthquake to ensure the impacts of this are documented and future studies can make informed decisions on which estimates to use (Table 1).

Sedimentary processes that may impact coseismic subsidence estimate variability

There are several second-order sedimentary processes that could potentially affect coseismic deformation estimates derived from microfossil-based quantitative RSL reconstructions from wetland stratigraphy, e.g. erosion, compaction, liquefaction and the sedimentation time lag for foraminiferal community re-establishment.

Erosion

Since erosion is the removal of material from a depositional environment, it is difficult to assess the amount of erosion that has taken place by investigating archived stratigraphy. Erosive processes, especially during storm surges and/or tsunami inundation, can remove material from an intertidal environment surface and/or transport foraminifera across tidal wetland environments. Subsequent deposition of transported foraminifera may create an assemblage with an allochthonous component that does not reflect the actual elevation of the sediment surface. For example, along a modern transect that crossed an eroding high-marsh block in Waikawa Harbor (NZ), Figueira and Hayward (2014) report 60–80% reworked high-marsh foraminifera at lower marsh elevations and up to 20% reworked tidal flat foraminifera at higher marsh elevations, which resulted in elevation estimates being 44–55 cm too high at lower tidal elevations and 25–42 cm too low at higher marsh elevations. Based on the modern transect with the reworked foraminifera, Figueira and Hayward (2014) go on to reconsider a previously recognised earthquake-related subsidence contact, found at nearby Catlins Lake, to be an eroded salt marsh collapsed block and not an earthquake-induced subsidence contact. Therefore, caution needs to be taken when deriving microfossil-based palaeotidal elevation estimates at locations where the modern salt marshes are exposed to erosive processes because erosion can cause both misleading biostratigraphy and tidal wetland stratigraphy.

During tsunami inundation, some erosion may be expected (Srinivasalu *et al.*, 2007; Switzer *and Jones*, 2008). However, tsunami deposits have not been documented at northern Humboldt Bay (e.g. Vick, 1988; Clarke and Carver, 1992; Valentine, 1992; Pritchard, 2004; Padgett *et al.*, 2021). Therefore, it is unlikely that northern Humboldt Bay salt marshes experienced tsunami inundation capable of eroding a salt-marsh peat unit. Stratigraphic mapping and radiocarbon age dating correlation results suggest that erosion may be responsible for an organic-rich unit missing at Jacoby Creek (Padgett *et al.*, 2021). However, given the highly localised extent, the erosion of this peat unit is likely the result of a migrating stream channel and not tsunami inundation.

Compaction and liquefaction

Compaction of a wetland stratigraphic sequence (e.g., Brain, 2015) may cause a lowering of a salt-marsh surface environment

in two ways: (1) auto-compaction of estuarine and marsh sediments in the absence of seismic shaking (Kemp et al., 2009, 2015; Brain et al., 2015, 2017); or (2) differential settlement induced by strong earthquake ground motions.

Although auto-compaction of organic-rich stratigraphy on the east coast of the United States (US) has been documented at several wetland sites (Brain et al., 2015; Kemp et al., 2015; Brain et al., 2017), it has not been studied along the active Cascadia margin. Along the east coast of the US, Holocene wetland environments accumulate continuous peat sections, which may be prone to compaction (Bloom, 1964; Allen, 2000; Brain et al., 2017). For a high-resolution sea-level reconstruction of a continuous peat record, stratigraphic compaction would result in an overestimation of the rate of sea-level rise (Brain et al., 2015). Along the Cascadia and other active tectonic margins, many wetland locations host a record of past relative sea-level changes over the late Holocene that is dominantly composed of minerogenic sediments with intercalated (and relatively thinner) organic-rich units, each of which also have the potential to auto-compact (Brain et al., 2011). However, such auto-compaction is not likely to affect the derivation of coseismic subsidence estimates for two reasons. Firstly, the critical information is the elevations at which the pre- and post-subsidence intervals formed and not the current elevation. In contrast, at passive margins, the current elevation of a stratigraphic interval is essential to the construction of long-term RSL histories (e.g. Kemp et al., 2015). Secondly, whilst compaction may result in a single-centimetre sediment slice covering a greater time period, the consistency of BTF estimates in the high marsh suggests this would not combine differing assemblages and, therefore, is unlikely to strongly influence the subsidence estimates.

Earthquake-induced compaction of the underlying Holocene coastal wetland stratigraphy at tidal wetlands has not been investigated at Cascadia. However, in much of Cascadia, the material underlying late Holocene coastal wetland stratigraphy is much older and should have already compacted because it has likely experienced 10+ earthquake cycles (e.g. Goldfinger et al., 2012). Therefore, compaction could potentially influence a coseismic subsidence estimate along the Cascadia margin and susceptibility increases if the salt marsh overlies an unconsolidated beach or dune sequence. However, such geological relationships are not the setting at the northern Humboldt Bay sites. We acknowledge that sediment deposited after the preceding earthquake that has not compacted through multiple seismic cycles could compact during the next earthquake prior to the resumption of sedimentation. The effect of this would be to increase a coseismic subsidence estimate. However, without the existence of geotechnical investigations at Cascadia we are unable to account for either earthquake-induced compaction of material underlying the stratigraphic sequence or compaction of rapidly deposited post-seismic material. This remains an area open for future investigations.

Post-seismic liquefaction in a salt marsh could affect the elevation of the salt-marsh platform (and, therefore, the estimate of coseismic subsidence from the BTF) in two ways: (1) surface elevation decreases due to the removal of the liquefied material underneath; or (2) surface elevation increases due to the subaerial deposition of ejected liquefied material, i.e. sand boils or blow (Clague et al., 1992; Quigley et al., 2013). Earthquake-induced liquefaction features have been documented along the Cascadia coastal margin at the Copalis River (Atwater, 1992), lower Columbia River (Atwater, 1994; Obermeier and Dickenson, 2000), at Sixes River, Oregon (Kelsey et al., 2002) and possibly at the Fraser River Delta in southwest Canada (Clague et al., 1992). It is possible

that shaking-related liquefaction could be attributed to variability of microfossil-derived coseismic vertical deformation estimates. However, no liquefaction features have been described in the stratigraphy at northern Humboldt Bay (Vick, 1988; Clarke and Carver, 1992; Valentine, 1992; Pritchard, 2004; Padgett et al., 2021). Therefore, we suggest that liquefaction is an unlikely second-order taphonomic process that may have affected our coseismic subsidence estimates.

Resumption of sedimentation

Wetland palaeogeodetic investigations cannot currently resolve the time duration of 'suddenness' of the resumption of sedimentation; therefore, coseismic subsidence estimates may contain post-seismic deformation (e.g. Nelson et al., 1996a; Atwater et al., 2001; Witter et al., 2003; Wang et al., 2013). Moreover, sedimentation may not be even across a marsh surface, e.g. the spatial extent and thickness of a deposit from channel levee overtopping, which could potentially explain differences in foraminiferal assemblages found in cores closely spaced, less than tens of metres. Both local ($1–2$ km^2) and estuary-wide ($\sim5–6$ km) rapid sedimentation can impact post-seismic stratigraphy, biostratigraphy and subsequent palaeoenvironmental interpretations (Atwater et al., 2001; Wang et al., 2013; Horton et al., 2017).

Even if post-seismic sedimentation resumed immediately after an earthquake, further complications can arise due to the microfossil response time. For example, foraminiferal response time was observed to be 11 months at a reclaimed marsh at Ni-les'tun marsh, Oregon, whereas diatom response time was observed to be 2 weeks (Horton et al., 2017). Therefore, different microfossils could under- or overestimate coseismic deformation (Horton et al., 2017). Even though the time of year of an earthquake could influence microfossil assemblages' response time, they are likely consistent across a marsh and estuary and are, therefore, unlikely to explain our observed inter- and intrasite coseismic subsidence variability.

Numerical possibilities for differences in coseismic subsidence estimates

Kemp et al. (2018) showed that RSL predictions were reasonably consistent regardless of training set and transfer function model choice. Given that our estimates are produced from the foraminiferal assemblages using the BTF, we must consider whether the statistical technique might be responsible for the observed variability. Possible numerical explanations might include count sizes and the composition of the modern training set.

The number of foraminifera tests counted for a stratigraphic interval can affect a RSL reconstruction, and resulting subsidence estimate, because taxa proportions could be inaccurate and/or misleading if the interval (depositional environment) is not adequately characterised. Kemp et al. (2020) suggest that count sizes of ~50 are likely to generate accurate reconstructions of earthquake-induced subsidence. Of our 170 cm interval counts, only four intervals have fewer than 50 individuals counted. Only one of the four intervals with fewer than 50 individuals counted were used in the derivation of a subsidence estimate, at *MD.06* for earthquake 2. However, despite a low count interval being used to produce a coseismic subsidence estimate at *MD.06*, we also found a nearly identical subsidence estimate at *MD.03*, 0.44 ± 0.35 cm and 0.42 ± 0.37 cm, respectively, suggesting that count size cannot explain the observed variability (Table 1). This result is consistent with the Kemp et al.

(2020) conclusion that with a count size of ~30 foraminifera, more than 95% of reconstructions are accurate.

An appropriate modern training set is critical to ensure confidence in the coseismic subsidence estimates produced by the BTF. Whilst there are some notable spatial gaps in the modern training set (e.g. Washington and northern California), the consistent elevation distribution of species between 32 and 50 degrees north (Kemp *et al.*, 2018) suggests that there is little scope for this to influence the results presented here. Our results suggesting that variability is driven by foraminiferal assemblages in the clastic sediments above the earthquake contact raise questions about the nature of the modern dataset and whether it contains an appropriate distribution of samples below MHHW. Investigation of the Kemp *et al.* (2018) dataset shows that there is a wide distribution of samples between ~75 and 200 SWLI. This is a suitable dataset given the lowest estimated SWLI midpoint of 115 SWLI (92.5 cm, *JC.06*). Kemp *et al.* (2018) noted that a transfer function developed only using the Oregon training set systematically overpredicted elevations below ~125 SWLI but that this effect was modest for transfer functions developed using the full west coast dataset employed here, which produced unbiased reconstructions. Therefore, we do not consider that the composition of the modern training set can explain the variability identified in this study.

Inherent intrasite coseismic subsidence variability and a sufficient number of reconstructions

In Oregon, palaeogeodetic investigations that apply the foraminiferal transfer function approach have reported ≤0.3 m of intrasite variability for the same subsidence contact (Milker *et al.*, 2016; Nelson *et al.*, 2020). Based on five separate subsidence contacts, Milker *et al.* (2016) report that at two core locations spaced 43 m apart, intrasite subsidence estimate variability ranges from 0.03 to 0.3 m per subsidence contact. Similarly, over a ~110 m distance, Nelson *et al.* (2020) found intrasite subsidence estimate variability to be 0.3 m for the 942–764 cal a BP subsidence contact. Similar results have also been found in Alaska (Shennan and Hamilton, 2006) with diatom-based transfer function subsidence estimates reproducible within the same marsh at cores 200–2500 m apart. Given our results across three subsidence contacts compare favourably with these earlier assessments, are in broad agreement with different microfossil groups, and across different sites, provides confidence in the quantitative microfossil-based approach. We found that over ~600–800 m distances intrasite coseismic subsidence estimate variability ranges from 0.01 to 0.32 m and averages ~0.1 m per each subsidence contact (Table 1). Therefore, the currently available data from Cascadia fossil foraminifera-based palaeogeodetic investigations suggest ≤0.3 m of inherent intrasite variability. Although our dataset cannot provide a definitive answer, the analyses of the extensive dataset presented here does suggest an approach to account for the seemingly inherent intrasite variability of foraminiferal-based coseismic subsidence estimates and highlights the potential role of physical mixing.

A challenge for testing the consistency of the RSL reconstructions and coseismic subsidence estimates is that unlike transplant experiments (e.g. Hamilton and Shennan, 2005; Engelhart *et al.* 2013a) we do not know the 'correct' answer. Instead, to gain confidence in an estuary-wide representative estimate, we derive multiple BTF coseismic subsidence estimate distributions across each marsh site for each earthquake contact and then assign an averaged intersite subsidence estimate as the representative subsidence value for the estuary (Table 1). Our analyses at northern Humboldt Bay lead us to suggest that by assessing

fossil assemblages at two to three core locations per subsidence contact per marsh site, we achieve convergence on a consistent estimate of coseismic subsidence. However, we also acknowledge that confidence in the significance of consistency will increase where different transfer functions (and different microfossils) may end up converging on the same result.

Implications for inferred heterogeneous rupture along strike for the CSZ 1700 CE earthquake, based on quantitative microfossil analyses

Given that recent megathrust ruptures showed non-uniform slip distributions (e.g. 2004 M_w 9.2 Sumatra–Andaman, 2010 M_w 8.8 Maule, Chile, 2011 M_w 9.0 Tohoku-Oki, Japan), it is likely that past Cascadia megathrust earthquakes also produced heterogeneous ruptures (e.g. Shennan *et al.*, 2016; Wang *et al.*, 2013). In Cascadia, much of our knowledge of past megathrust slip distribution is derived from microfossil analysis of coastal stratigraphic records (e.g. Witter *et al.*, 2012; Wang *et al.*, 2013; Kemp *et al.*, 2018; Nelson *et al.*, 2020). Therefore, when considering past megathrust rupture and possible heterogeneous slip distributions, it is critical to avoid misinterpreting stratigraphic and biostratigraphic data. For example, given the margin-wide, fossil-foraminifera-derived subsidence estimates within the CSZ palaeogeodetic database for the 1700 CE earthquake of Kemp *et al.* (2018), there are low subsidence estimates adjacent to high subsidence estimates. For example, Netarts Bay has a low amount of subsidence (0.39 ± 0.20 m), but Nehalem River 17.5 km to the north has a high amount of subsidence (1.16 ± 0.21 m) and Nestucca River, which is 24 km south of Netarts Bay, has a similarly large amount of subsidence (1.09 ± 0.46 m). Does the along-strike heterogeneity of coseismic vertical deformation estimates reflect variable slip on the megathrust or could such differences be the result of biostratigraphic and/or stratigraphic variability?

At northern Humboldt Bay, we observed up to 0.76 m of intersite variability between coseismic subsidence estimates for the 1700 CE earthquake (Table 1). We draw confidence in our estuary-wide average estimate, of 0.81 ± 0.19 m, by replicating the approach of deriving a subsidence estimate at nine locations over a > 6 km transect and subsequently removing three estimates from a marsh site with mixed biostratigraphy (Mad River Slough; Table 1; Fig. 3; Tables S1–S9, Figs S1–S3). A worst-case scenario would be to assign an estuary-wide subsidence estimate based on only one reconstruction from either end of our subsidence estimate range, 0.24 ± 0.27 m to 1.00 ± 0.44 m. On a margin-wide scale, a 0.76 m difference from any subsidence estimate could potentially remove or create reason to infer variable slip on the megathrust.

Within the CSZ 1700 CE palaeogeodetic database of Kemp *et al.* (2018), subsidence estimates range from a minimum of 0.16 ± 0.21 m at Alsea Bay to a maximum of 1.41 ± 0.43 m at Salmon River (Kemp *et al.*, 2018). Given the variability of transfer function subsidence estimates, does this suggest that the lowest estimates, which are at Netarts Bay (0.39 ± 0.20 m) and Alsea Bay, could be anomalous coseismic subsidence estimates? We argue that this is unlikely because at each site, Netarts and Alsea, there are two intrasite microfossil estimates with errors that overlap, even though one is a non-transfer function estimate. At Netarts, a quantitative pollen and diatom RSL reconstructions suggest 0.4 ± 0.3 m of subsidence (Shennan *et al.*, 1998), supported by a foraminiferal BTF reconstruction that suggests 0.39 ± 0.20 m subsidence (Kemp *et al.*, 2018). At Alsea Bay, two foraminiferal transfer function estimates are 0.13 ± 0.21 (Nelson *et al.*, 2008) and 0.16 ± 0.32 m (Wang *et al.*, 2013), and are further supported by a local diatom-based transfer function estimate of 0.16 ± 0.12 m (Nelson *et al.*, 2008). Therefore,

multiple microfossil reconstructions substantiate subsidence estimates. Prior to this investigation, Alsea and Netarts were outliers within the palaeogeodetic database because they were the only locations with more than one microfossil-based RSL reconstruction for the 1700 CE earthquake. However, at Alsea and Netarts, the estimates are intrasite replications and, therefore, cannot account for the possibility of intersite variability. To fully account for intersite variability within an estuary, wherever possible each Cascadia margin estuary site should have at least two (replicate) microfossil-derived quantitative subsidence analyses per contact. Given that our results support previous analyses suggesting that intrasite variability is limited and within analytical uncertainty, priority should be given to obtaining at least two (replicate) microfossil-derived quantitative subsidence analyses per contact from different sites within an estuary to assess intersite variability. This will provide greater confidence in future interpretations of slip heterogeneity due to along-strike variation in coseismic subsidence.

CONCLUSIONS

It is critical that palaeogeodetic investigations account for tidal wetland stratigraphic variability and avoid a misrepresentation of coseismic deformation when variability may be more intrinsic to factors affecting local microfossil assemblages and not reflective of actual variation in rupture characteristics along-strike of a subduction zone. Furthermore, coastal palaeogeodetic investigations select stratigraphic sequences that display the most visually abrupt contact for microfossil analyses. However, our data document variability within tidal wetland stratigraphy that may not be discernable via in-field optical inspection and only recognised after laboratory analysis.

Prior to our investigation, no work has focused on assessing the reproducibility of microfossil-based transfer function coseismic deformation estimates over distances of 1–6 km across multiple tidal marshes in the same estuarine system. Therefore, we constructed a database of 20 (fossil foraminifera BTF-derived) subsidence estimates, which contains 5–9 RSL reconstructions across three subsidence contacts and three marshes. Fossil foraminiferal assemblages, BTF analysis (Kemp et al., 2018) and sediment core density imagery combine to highlight stratigraphic variability within an individual marsh and across multiple marshes within the estuary. Our robust analysis allows us to: (1) quantify inherent intrasite variability of coseismic subsidence estimates; (2) identify mixed deposition above the 1700 CE contact at Mad River Slough; and (3) determine that intrasite variability is primarily driven by foraminiferal assemblages within the mud units overlying the earthquake-induced subsidence contact.

Our case study across three coseismic subsidence contacts at northern Humboldt Bay demonstrates that replicated RSL reconstructions and stratigraphic analyses can refine our understanding of tidal wetland stratigraphic variability and suggest improvements to coastal palaeogeodetic research approaches. Based on our estuary-wide survey of high-resolution biostratigraphic and lithostratigraphic data, we conclude that site-specific stratigraphic inconsistencies and inherent intrasite variability can be accounted for within the derivation of an intersite averaged subsidence estimate (i.e. multiple marshes within an estuary). These results have broad implications for the development of quantitative, microfossil-based coseismic subsidence estimates at global subduction zones. Based on our findings, we suggest that researchers can avoid palaeoenvironmental misrepresentation by assessing

biostratigraphy and lithostratigraphy at a minimum of two spread-out core locations per contact and, wherever possible, across multiple marshes within an estuary.

Supporting information

Additional supporting information may be found in the online version of this article at the publisher's web-site.
  Supporting information.

REFERENCES

Allen JR. 2000. Morphodynamics of Holocene salt marshes: A review sketch from the Atlantic and Southern North Sea coasts of Europe. *Quaternary Science Reviews* **19**: 1155–1231.

Atwater BF. 1987. Evidence for great Holocene earthquakes along the outer coast of Washington State. *Science* **236**: 942–944.

Atwater BF. 1992. Geologic evidence for earthquakes during the past 2000 years along the Copalis River, southern coastal Washington. *Journal of Geophysical Research: Solid Earth* **97**: 1901–1919.

Atwater BF. 1994. *Geology of Holocene liquefaction features along the lower Columbia River at Marsh, Brush, Price, Hunting, and Wallace Islands, Oregon and Washington* (No. 94-209). US Geological Survey.

Atwater BF, Hemphill-Haley E. 1997. *Recurrence intervals for great earthquakes of the past 3,500 years at northeastern Willapa Bay, Washington* (No. 1576). USGPO; Information Services [distributor].

Atwater BF, Yamaguchi DK, Bondevik S et al. 2001. Rapid resetting of an estuarine recorder of the 1964 Alaska earthquake. *Geological Society of America Bulletin* **113**: 1193–1204.

Bloom AL. 1964. Peat accumulation and compaction in a Connecticut coastal marsh. *Journal of Sedimentary Research* **34**: 599–603.

Brain MJ. 2015. Compaction. In *Handbook of Sea-Level Research*, Shennan I, Long AJ, Horton BP (eds). John Wiley & Sons, 452–469.

Brain MJ, Long AJ, Petley DN et al. 2011. Compression behaviour of minerogenic low energy intertidal sediments. *Sedimentary Geology* **233**: 28–41.

Brain MJ, Kemp AC, Hawkes AD et al. 2017. Exploring mechanisms of compaction in salt-marsh sediments using Common Era relative sea-level reconstructions. *Quaternary Science Reviews* **167**: 96–111.

Brain MJ, Kemp AC, Horton BP, Culver SJ, Parnell AC, Cahill N. 2015. Quantifying the contribution of sediment compaction to late Holocene salt-marsh sea-level reconstructions, North Carolina, USA. *Quaternary Research* **83**: 41–51.

Briggs RW, Engelhart SE, Nelson AR et al. 2014. Uplift and subsidence reveal a nonpersistent megathrust rupture boundary (Sitkinak Island, Alaska). *Geophysical Research Letters* **41**: 2289–2296.

Cahill N, Kemp AC, Horton BP et al. 2016. A Bayesian hierarchical model for reconstructing relative sea level: from raw data to rates of change. *Climate of the Past* **12**: 525–542.

Cisternas M, Atwater BF, Torrejón F et al. 2005. Predecessors of the giant 1960 Chile earthquake. *Nature* **437**: 404.

Clague JJ, Naesgaard E, Sy A. 1992. Liquefaction features on the Fraser delta: evidence for prehistoric earthquakes? *Canadian Journal of Earth Sciences* **29**: 1734–1745.

Clarke SH, Carver GA. 1992. Late Holocene tectonics and paleoseismicity, southern Cascadia subduction zone. *Science* **255**: 188–192.

Combellick RA. 1991. *Paleoseismicity of the Cook Inlet region, Alaska: Evidence from peat stratigraphy in Turnagain and Knik Arms* (No. 112). State of Alaska, Department of Natural Resources, Division of Geological & Geophysical Surveys.

Darienzo ME, Peterson CD, Clough C. 1994. Stratigraphic evidence for great subduction-zone earthquakes at four estuaries in northern Oregon, USA. *Journal of Coastal Research*: 850–876.

Davies MH, Mix AC, Stoner JS et al. 2011. The deglacial transition on the southeastern Alaska Margin: Meltwater input, sea level rise, marine productivity, and sedimentary anoxia. *Paleoceanography and Paleoclimatology* **26**(2): PA2223.

de Rijk S. 1995. Salinity control on the distribution of salt marsh foraminifera (Great Marshes, Massachusetts). *The Journal of Foraminiferal Research* **25**: 156–166.

Dura T, Horton BP, Cisternas M et al. 2017. Subduction zone slip variability during the last millennium, south-central Chile. *Quaternary Science Reviews* **175**: 112–137.

Eicher AL. 1987. *Salt marsh vascular plant distribution in relation to tidal elevation, Humboldt Bay, California* [M.S. thesis]. Arcata, California, Humboldt State University.

Engelhart SE, Horton BP, Nelson AR et al. 2013a. Testing the use of microfossils to reconstruct great earthquakes at Cascadia. *Geology* **41**: 1067–1070.

Engelhart SE, Horton BP, Vane CH et al. 2013b. Modern foraminifera, δ 13 C, and bulk geochemistry of central Oregon tidal marshes and their application in paleoseismology. *Palaeogeography, Palaeoclimatology, Palaeoecology* **377**: 13–27.

Engelhart SE, Hemphill-Haley E, Kelsey HM et al. 2016. *Refined Estimates of Coseismic Subsidence along the Southern Cascadia Subduction Zone in Northern Humboldt Bay (Arcata Bay).* U.S. Geological Survey Grant Report, Collaborative Research with University of Rhode Island and Humboldt State University, No. G14AP00128 and G14AP00129. U.S. Geological Survey. Final Technical Report.

Figueira B, Hayward BW. 2014. Impact of reworked foraminifera from an eroding salt marsh on sea-level studies, New Zealand. *New Zealand Journal of Geology and Geophysics* **57**: 378–389.

Fuglede B, Topsoe F. 2004. June. Jensen-Shannon divergence and Hilbert space embedding. In *International Symposium on Information Theory (ISIT) 2004. Proceedings.* IEEE; 31.

Garrett E, Shennan I, Woodroffe SA et al. 2015. Reconstructing paleoseismic deformation, 2: 1000 years of great earthquakes at Chucalén, south central Chile. *Quaternary Science Reviews* **113**: 112–122.

Goldfinger C, Nelson CH, Morey A et al. 2012, *Turbidite event history —Methods and implications for Holocene paleo-seismicity of the Cascadia subduction zone.* U.S. Geological Survey Professional Paper 1661-F. https://doi.org/10.3133/pp1661F

Guilbault JP, Clague JJ, Lapointe M. 1995. Amount of subsidence during a late Holocene earthquake—evidence from fossil tidal marsh foraminifera at Vancouver Island, west coast of Canada. *Palaeogeography, Palaeoclimatology, Palaeoecology* **118**: 49–71.

Guilbault JP, Clague JJ, Lapointe M. 1996. Foraminiferal evidence for the amount of coseismic subsidence during a late Holocene earthquake on Vancouver Island, west coast of Canada. *Quaternary Science Reviews* **15**: 913–937.

Hamilton S, Shennan I. 2005. Late Holocene relative sea-level changes and the earthquake deformation cycle around upper Cook Inlet, Alaska. *Quaternary Science Reviews* **24**: 1479–1498.

Hawkes AD, Horton BP, Nelson AR et al. 2010. The application of intertidal foraminifera to reconstruct coastal subsidence during the giant Cascadia earthquake of AD 1700 in Oregon, USA. *Quaternary International* **221**: 116–140.

Hawkes AD, Horton BP, Nelson AR et al. 2011. Coastal subsidence in Oregon, USA, during the giant Cascadia earthquake of AD 1700. *Quaternary Science Reviews* **30**: 364–376.

Holden PB, Birks HJB, Brooks SJ et al. 2017. BUMPER v1. 0: a Bayesian user-friendly model for palaeo-environmental reconstruction.

Horton BP, Edwards RJ. 2006. Quantifying Holocene Sea Level Change Using Intertidal Foraminifera: Lessons from the British Isles. *Cushman Foundation for Foraminiferal Research Special Publication* **40**.

Horton BP, Milker Y, Dura T et al. 2017. Microfossil measures of rapid sea-level rise: Timing of response of two microfossil groups to a sudden tidal-flooding experiment in Cascadia. *Geology* **45**: 535–538.

Kemp AC, Horton BP, Culver SJ et al. 2009. Timing and magnitude of recent accelerated sea-level rise (North Carolina, United States). *Geology* **37**: 1035–1038.

Kemp AC, Telford RJ. 2015. Transfer functions. In *Handbook of Sea-Level Research.*, Shennan I, Long AJ, Horton BP (eds). John Wiley and Sons: Chichester; 470–499.

Kelsey HM, Witter RC, Hemphill-Haley E. 2002. Plate-boundary earthquakes and tsunamis of the past 5500 yr, Sixes River estuary, southern Oregon. *Geological Society of America Bulletin* **114**: 298–314.

Kemp AC, Hawkes AD, Donnelly JP et al. 2015. Relative sea-level change in Connecticut (USA) during the last 2200 yrs. *Earth and Planetary Science Letters* **428**: 217–229.

Kemp AC, Cahill N, Engelhart SE et al. 2018. Revising Estimates of Spatially Variable Subsidence during the AD 1700 Cascadia Earthquake Using a Bayesian Foraminiferal Transfer Function. *Bulletin of the Seismological Society of America* **108**: 654–673.

Kemp AC, Wright AJ, Cahill N. 2020. Enough is enough or more is more? Testing the influence of foraminiferal count size on reconstructions of paleomarsh elevation. *Journal of Foraminiferal Research* **50**: 266–278.

Menéndez ML, Pardo JA, Pardo L, Pardo MC. 1997. The jensen-shannon divergence. *Journal of the Franklin Institute*, **334**(2), 307–318.

Milker Y, Horton BP, Vane CH et al. 2015. Annual and seasonal distribution of intertidal foraminifera and stable carbon isotope geochemistry, Bandon Marsh, Oregon, USA. *The Journal of Foraminiferal Research* **45**: 146–155.

Milker Y, Nelson AR, Horton BP et al. 2016. Differences in coastal subsidence in southern Oregon (USA) during at least six prehistoric megathrust earthquakes. *Quaternary Science Reviews* **142**: 143–163.

Nelson AR. 1992. Discordant 14 C ages from buried tidal-marsh soils in the Cascadia subduction zone, southern Oregon coast. *Quaternary Research* **38**: 74–90.

Nelson AR, Shennan I, Long AJ. 1996a. Identifying coseismic subsidence in tidal-wetland stratigraphic sequences at the Cascadia subduction zone of western North America. *Journal of Geophysical Research: Solid Earth* **101**: 6115–6135.

Nelson AR, Jennings AE, Kashima K. 1996b. An earthquake history derived from stratigraphic and microfossil evidence of relative sea-level change at Coos Bay, southern coastal Oregon. *Geological Society of America Bulletin* **108**: 141–154.

Nelson AR, Sawai Y, Jennings AE et al. 2008. Great-earthquake paleogeodesy and tsunamis of the past 2000 years at Alsea Bay, central Oregon coast, USA. *Quaternary Science Reviews* **27**: 747–768.

Nelson AR, Hawkes AD, Sawai Y et al. 2020. Identifying the greatest earthquakes of the past 2000 years at the Nehalem River Estuary, northern Oregon Coast, USA. *OpenQuaternary* **6**: 1–30.

Obermeier SF, Dickenson SE. 2000. Liquefaction evidence for the strength of ground motions resulting from late Holocene Cascadia subduction earthquakes, with emphasis on the event of 1700 AD. *Bulletin of the Seismological Society of America* **90**: 876–896.

Padgett JS, Engelhart SE, Kelsey HM et al. 2021. Timing and amount of southern Cascadia earthquake subsidence over the past 1700 years at northern Humboldt Bay, California, USA. *GSA Bulletin* **133**: 2137–2156.

Pickart AJ, Hesp PA. 2019. Spatio-temporal geomorphological and ecological evolution of a transgressive dunefield system, Northern California, USA. *Global and planetary change* **172**: 88–103.

Plafker G. 1969. *Tectonics of the March 27, 1964, Alaska earthquake.* U.S. Geological Survey Professional Paper 543-I.

Pritchard CJ. 2004. *Late Holocene relative sea-level changes, Arcata Bay, California: Evaluation of freshwater syncline movement using*

coseismically buried soil horizons [M.S. thesis]. Humboldt State University Arcata, CA.

Quigley MC, Bastin S, Bradley BA. 2013. Recurrent liquefaction in Christchurch, New Zealand, during the Canterbury earthquake sequence. *Geology* **41**: 419–422.

Rothwell RG, Rack FR. 2006. New techniques in sediment core analysis: an introduction. *Geological Society, London, Special Publications* **267**: 1–29.

Sawai Y, Nasu H, Yasuda Y. 2002. Fluctuations in relative sea-level during the past 3000 yr in the Onneth estuary, Hokkaido, northern Japan. *Journal of Quaternary Science* **17**: 607–622.

Schlosser S, Eicher A. 2012. *The Humboldt Bay and Eel River Estuary Benthic Habitat Project*. California Sea Grant Publication T-075.

Scott DB, Medioli FS. 1980. Living vs. total foraminiferal populations: their relative usefulness in paleoecology. *Journal of Paleontology* **54**: 814–831.

Shennan I, Long AJ, Rutherford MM *et al*. 1996. Tidal marsh stratigraphy, sea-level change and large earthquakes, I: a 5000 year record in Washington, USA. *Quaternary Science Reviews* **15**: 1023–1059.

Shennan I, Scott DB, Rutherford M *et al*. 1999. Microfossil analysis of sediments representing the 1964 earthquake, exposed at Girdwood Flats, Alaska, USA. *Quaternary International* **60**: 55–73.

Shennan I, Hamilton S. 2006. Coseismic and pre-seismic subsidence associated with great earthquakes in Alaska. *Quaternary Science Reviews* **25**: 1–8.

Shennan I, Barlow N, Combellick R *et al*. 2014. Late Holocene paleoseismology of a site in the region of maximum subsidence during the 1964 Mw 9.2 Alaska earthquake. *Journal of Quaternary Science* **29**: 343–350.

Shennan I, Garrett E, Barlow N. 2016. Detection limits of tidal-wetland sequences to identify variable rupture modes of megathrust earthquakes. *Quaternary Science Reviews* **150**: 1–30.

Shennan I, Long AJ, Rutherford MM, Innes JB, Green FM, Walker KJ. 1998. Tidal marsh stratigraphy, sea-level change and large earthquakes—II: submergence events during the last 3500 years at Netarts Bay, Oregon, USA. *Quaternary Science Reviews*, **17**(4-5), 365–393.

Srinivasalu S, Thangadurai N, Switzer AD *et al*. 2007. Erosion and sedimentation in Kalpakkam (N Tamil Nadu, India) from the 26th December 2004 tsunami. *Marine Geology* **240**: 65–75.

Switzer AD, Jones BG. 2008. Large-scale washover sedimentation in a freshwater lagoon from the southeast Australian coast: sea-level change, tsunami or exceptionally large storm? *The Holocene* **18**: 787–803.

Thompson RW. 1971. Recent sediments of Humboldt Bay. *Eureka, California, final report. Petroleum Research Fund* **789**: G2.

Valentine DW. 1992. *Late Holocene stratigraphy, Humboldt Bay, California: Evidence for late Holocene paleoseismicity of the southern Cascadia subduction zone* [M.S. thesis]. Humboldt State University, Arcata, CA.

Vick GS. 1988. *Late Holocene paleoseismicity and relative sea level changes of the Mad River Slough, northern Humboldt Bay, California* [M.S. thesis]. Humboldt State University, Arcata, CA.

Wang PL, Engelhart SE, Wang K *et al*. 2013. Heterogeneous rupture in the great Cascadia earthquake of 1700 inferred from coastal subsidence estimates. *Journal of Geophysical Research: Solid Earth* **118**: 2460–2473.

Witter RC, Kelsey HM, Hemphill-Haley E. 2003. Great Cascadia earthquakes and tsunamis of the past 6700 years, Coquille River estuary, southern coastal Oregon. *Geological Society of America Bulletin* **115**: 1289–1306.

Witter RC, Zhang Y, Wang K *et al*. 2012. Coseismic slip on the southern Cascadia megathrust implied by tsunami deposits in an Oregon lake and earthquake-triggered marine turbidites. *Journal of Geophysical Research* **117**: B10303.

Witter R, Briggs R, Engelhart SE *et al*. 2019. Evidence for frequent, large tsunamis spanning locked and creeping parts of the Aleutian megathrust. *Geological Society of America Bulletin* **131**: 707–729.